INTERACTIONS BETWEEN AZA-ENEDIYNES AND PROTEINS

THESIS

Presented to the Graduate Council
of Texas State University–San Marcos
in Partial Fulfillment
of the Requirements

for the Degree

Master of SCIENCE

by

Cristina Gonzales, B.S.

San Marcos, Texas
May 2006

ACKNOWLEDGEMENTS

The past two years have been a great experience and a pursuit for knowledge. However, the outcome would not have been possible without the love and support of many. I have learned that this world is filled with people who will go out of their way to lend a helping hand.

I would like to, first and foremost, thank the Lord who strengthens me and who has introduced me to a wonderful family, friends, and professors.

I am grateful for the support for my family and the strong work ethic they have instilled in me.

I have been blessed with great friends. Thanks to Esteban Cortez and Alison Russell for their encouragement and friendship.

I would like to extend my deepest appreciation to my committee: Dr. Lewis; Dr. Booth; and my advisor, Dr. David. Thank you, Dr. Lewis for being my mentor and professor. You are hard working, dedicated, and committed to your students. Dr. David, thank you for your support. I would not have been able to work in any other lab because I am truly interested in your area of research. I would also like to extend my gratitude to Dr. Beall, who does not happen to be a part of my committee. Although he is the busiest most industrious person, he always dropped what was doing to listen and be of assistance to me.

TABLE OF CONTENTS

LIST OF TABLES

LIST OF FIGURES

FIGURE **PAGE**

CHAPTER I

INTRODUCTION

1. Enediyne Natural Products and Aza-Enediynes

Enediynes are naturally occurring antitumor, antibiotic natural products. Upon activation enediynes are known to generate diradical structures that abstract hydrogens from the DNA backbone, leading to DNA scission (1). The diradical structure is generated via a Bergman cyclization (Figure 1) (2). The Bergman cyclization of simple, acyclic enediynes requires temperatures near 200 °C; however, most naturally occurring enediynes possess elaborate triggering mechanisms to facilitate the cyclization. A variety of compounds have been classified as antitumor drugs due to their common enediyne core, of which several structures are shown in Figure 2 (3-8).

The potency of enediynes *in vivo* has been demonstrated to correlate with the ability of enediynes to cleave DNA. For instance, the introduction of calechemicin into yeast cells induces an upregulation of the genes involved in DNA repair (9). Neocarzinostatin (zinostatin, NCS), an enediyne natural product, is known to induce double stand breaks (DSB's) in Chinese hamster ovary (CHO) cells (10). The instability of zinostatin indicates that the cleavage occurs within a few hours of exposure to the cells (10).

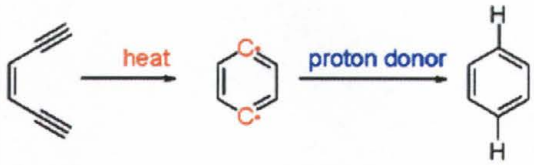

Figure 1. Bergman cyclization of enediynes.

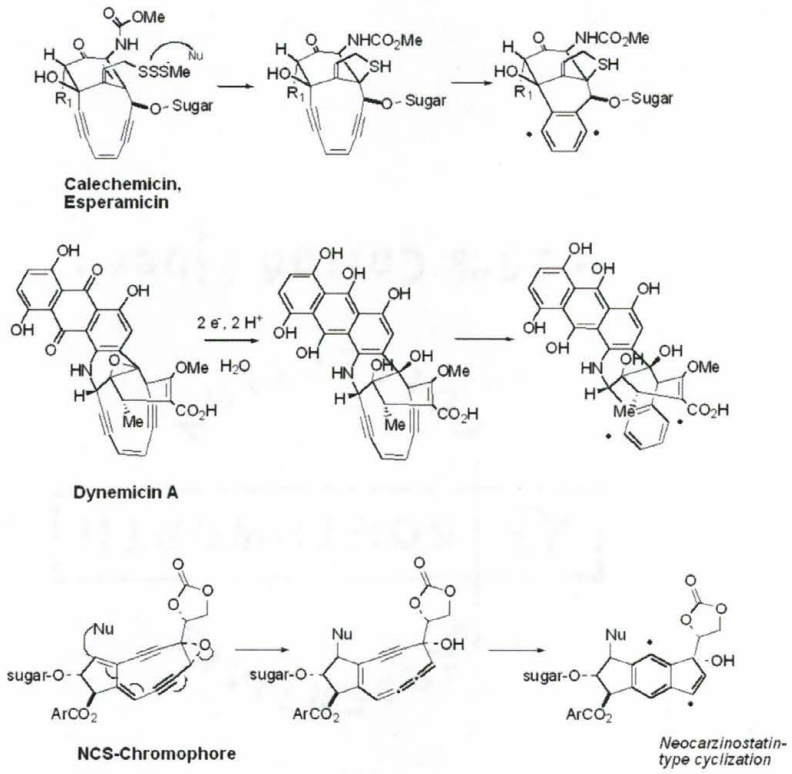

Figure 2. Naturally occurring calechemicin, esperamicin, dynemicin, and NCS-Chromophore, which contain the core enediyne structure.

Enediynes have been widely studied due to their potency and ability to act as antitumor agents, however, their use is limited because of their toxicity. Consequently, the development of synthetic enediynes with improved properties has received wide interest (11,12).

Aza-enediynes, synthetic analogs of enediynes, have been synthesized by Kerwin and coworkers at the University of Texas in an effort to generate compounds that undergo cyclization more readily under physiological conditions (13-16). Aza-enediynes have a characteristic C=N that replaces the C=C present in enediynes and undergo analogous cyclizations to generate reactive intermediates (Figure 3). Although aza-enediynes form reactive intermediates that may participate in DNA cleavage (16), the interaction of aza-enediynes with proteins has not been studied previously and is the focus of the research presented.

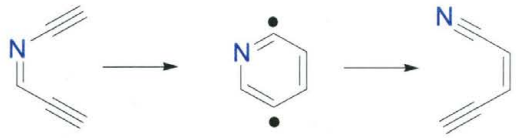

Figure 3. Aza-Bergman rearrangement of aza-enediynes.

2. Potential Interactions Between Aza-Enediynes and Proteins

In the presence of a protein, the reactive pyridine-based diradical formed during aza-Bergman rearrangement of an aza-enediyne (shown above in Figure 3) may utilize the protein as a hydrogen atom source. The result of this interaction would most likely

lead to amino acid side-chain oxidation, and the resulting products would be difficult to characterize.

However, other reactive aza-enediyne intermediates may form and be capable of interaction with protein or peptide targets. Some types of aza-enediynes cyclize to generate carbenes (Figure 4) (14). The resulting carbene product is highly reactive, but is likely persistent enough to undergo insertion or hydrogen-atom abstraction reactions in water. This is not without precedent, since phenylurea-derived carbenes have also been shown to be fairly persistent in an aqueous environment (17). The potential carbenes generated by aza-enediynes would be expected to undergo insertion reactions with amino acid side-chains, particularly those of tryptophan and phenylalanine. If a carbene inserts into the electron-rich phenyl ring of phenylalanine, for instance, the product shown in Figure 4 would result.

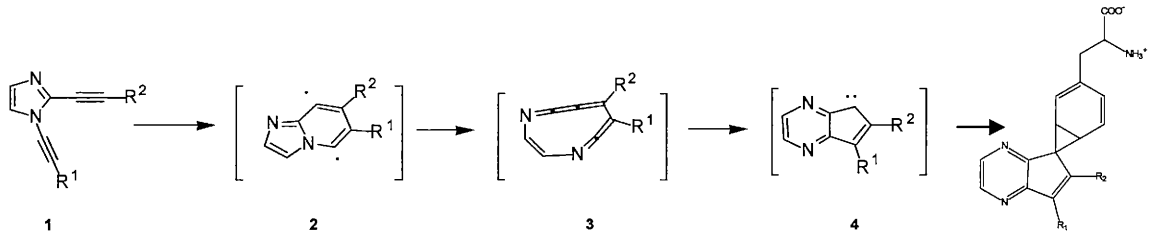

Figure 4. Cyclization of aza-enediynes capable of forming carbene intermediates.

Another potential interaction that may occur between aza-enediynes and proteins or peptides involves nucleophilic attack on the alkyne moieties (i.e., from a protein thiol or amine group serving as the nucleophile, Nu) (Figure 5).

The product shown in Figure 5 would result from nucleophilic attack of a lysine side-chain amino group onto the upper alkyne portion of the aza-enediyne. Cysteine, lysine, serine, threonine, and tyrosine amino acid side-chains would be the most likely participants in this type of modification. In this case, as for carbene insertion, the protein would become covalently modified with the aza-enediyne.

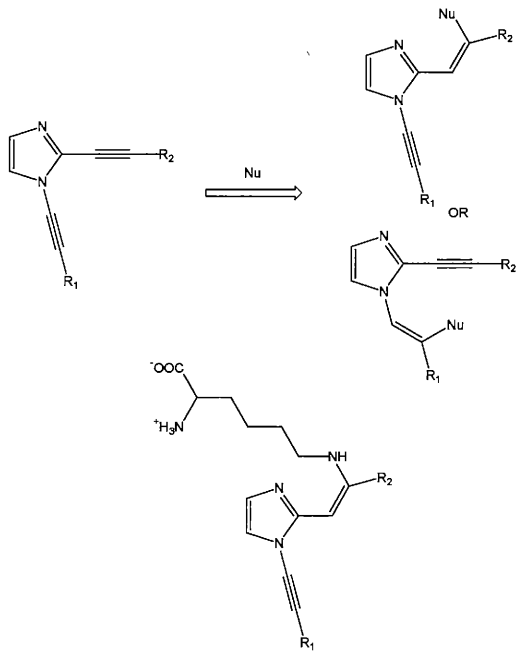

Figure 5. Nucleophilic attack on the alkyne moieties of aza-enediynes.

3. Targeting p38α with Aza-Enediynes

In addition to the general modifications of amino acid components mentioned above that may occur with any protein, several aza-enediynes may serve as inhibitors of p38α since they possess some similarities in structure to known inhibitors, such as SB-203580 and RWJ 67657 (Figure 6). For instance, RWJ 67657 has an alkynyl-substituted

imidazole, which is present in aza-enediynes KeAZB-104A, KeAZB-106, and KeAZB-037. In contrast, the pyridyl and *p*-fluorophenyl substituents of RWJ 67657 and SB-203580 are absent from aza-enediynes.

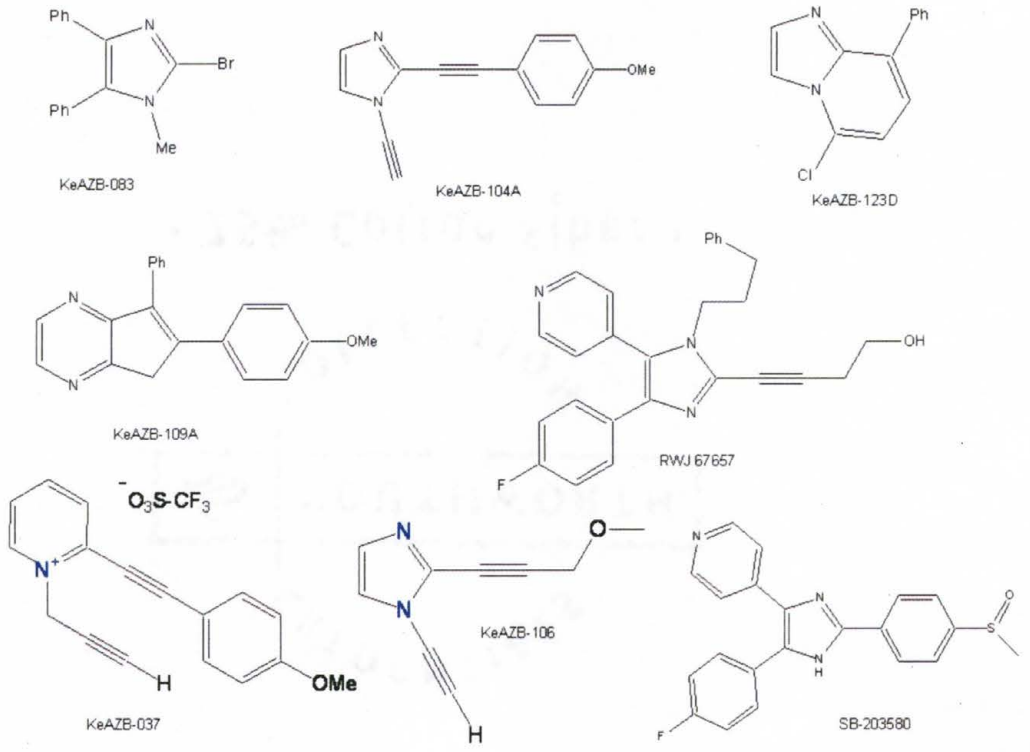

Figure 6. Aza-enediynes and two known inhibitors of p38 (SB-203580 and RWJ67675).

The inhibition of p38α is being studied in order to control diseases that cause excessive inflammation such as rheumatoid arthritis, osteoporosis, and inflammatory bowel disease (18). P38α is a mitogen-activated protein kinase (MAPK) that belongs to a conserved family of protein kinases, members of which are important in controlling cellular responses to inflammation and growth signals, apoptosis, and the directionality of

cell migration by distinct mechanisms (19-21). Activation of p38α by upstream MAPKs occurs in response to inflammatory stimuli and can be induced by environmental stresses such as osmotic shock and UV light (22). Once activated, p38α phosphorylates various downstream MAPKs and transcription factors, ultimately leading to the production of a number of important cytokines, including tumor necrosis factor alpha (TNFα) and interleukin-1beta (IL-1β).

Most p38α inhibitors compete with ATP binding. Crystallographic analyses of kinases with ATP bound reveal that the N-terminal domain forms a binding site for the adenine ring of ATP, and the C-terminal domain presents a binding site for magnesium, the β-phosphate of ATP, and the catalytic base (23). The two domains play a critical role in creating a pocket for binding substrates. Using a competitive binding assay, the interaction between p38 and ATP was measured, and results suggest that ATP is unable to bind inactive p38. The inactive form of p38 has domains that are misaligned; therefore ATP is unable to bind, and no kinase activity is present (23).

Many competitive inhibitors of ATP binding to p38α, including SB-203580 and RWJ 67657, also bind to *inactive* p38α as noncompetitive inhibitors of ATP binding. It is likely that these inhibitors keep inactive p38α from activating downstream kinases. (24). Kinetic studies of the binding of several small inhibitor molecules to p38 using surface plasmon resonance have been used to determine dissociation constants, important information for evaluating the potency and efficacy of inhibitors (24-25). Dissociation constants for the specific binding of reversible inhibitors SB-203580 and RWJ 67657 to p38α (K_d = 22 nm and 10 nm, respectively) correlate to their IC_{50} values for the

inhibition of TNFα expression (24). Both these inhibitors, however, have similar association rates of 8 X 10^5 $M^{-1} \cdot s^{-1}$.

4. Experimental Approach

In order to determine the potential for aza-enediynes to interact with proteins either through carbene insertion reactions or nucleophilic addition, a model protein (bovine serum albumin, BSA) and small peptide (bradykinin) was incubated with aza-enediynes. BSA was chosen as a model because it is a well-characterized protein and is readily available. Bradykinin has two phenylalanine residues that may serve as carbene insertion sites and a serine residue (potential nucleophile), in addition to the N-terminus. Aza-enediynes were incubated with BSA and bradykinin and subsequently analyzed for potential modifications using either gel electrophoresis or matrix-assisted-laser-desorption time-of-flight mass spectrometry (MALDI-TOF-MS).

Additionally, the potential for aza-enediynes to bind p38α was analyzed using molecular modeling. Molecular modeling is a tool used to obtain structural information such as bond angles or bond lengths, study the interaction between molecules, and determine heats of formation. Molecular modeling programs such as the commercially available Cerius 2 software package are commonly used to determine the structure of protein complexes with accuracy similar to that provided by X-ray crystallography data (26). Modeling proteins is a useful tool for structure-based drug design. Not only does the modeling tool provide a visualization technique, but it is useful for advanced calculations.

Protein-protein docking allows the computational determination of protein 3D structural interactions. Protein molecules dock with one another in order to function as inhibitors or activators. Drugs function by docking with proteins and interfering with

their ability to function (27). Protein docking allows the prediction of protein interactions that can then be compared to experimental measurement. Protein-protein docking may answer questions about the spatial configurations proteins adopt while ligands or inhibitors are bound, as well as the strength of protein interactions.

Accelrys' Cerius 2 software (modeling program) was used to model the interaction between p38 and potential inhibitor molecules such KeAZB-037, KeAZB-083, KeAZB-104, KeAZB-106, and KeAZB-109. The structure of p38α in complex with a small molecule inhibitor was imported from the Protein Data Bank (obtained from crystal data, PDB id 1W7H) and used to determine the active site configuration (28). The interactions were studied and compared to the energy values of the known inhibitor 3-(benzyloxy) pyridin-2-amine, previously analyzed by Hartshorn *et al.* (28).

Finally, using bimolecular interaction analysis (BIA), with Biacore's surface plasmon resonance (SPR) technology, the interaction between several aza-enediynes and p38 was determined. Biacore studies provide information about the interaction of potential drug candidates (typically less than 1000 Da) with a target molecule. The kinetics, specificity, and affinity of an analyte for a particular ligand can be measured without the use of labels. Suface plasmon resonance (SPR) measures the binding of molecules in real-time. The measurement of binding interactions between molecules can be achieved by immobilizing a target molecule to a sensor chip surface and passing the binding partners over the sensor chip (29). In our case, p38 was directly coupled to the sensor chip and reversibly stabilized with the use of a co-ligand.

In summary, various approaches were utilized to measure the interactions of aza-enediynes with proteins. Gel electrophoresis, biomolecular interactions determined by

SPR, mass spectrometry, and molecular modeling experiments provided preliminary information about the interactions of aza-enediynes with proteins. The information obtained may be helpful in assessing the ability of aza-enediynes to function as inhibitors of p38α and modify proteins in general.

CHAPTER 2

MATERIALS AND METHODS

I. MATERIALS

General Reagents

Sodium chloride was purchased from Mallinckrodt AR (Paris, Kentucky). Ethidium bromide was purchased from Shelton Scientific, Incorporated (Shelton, CT). Bovine Serum Albumin (BSA) and dimethyl sulfoxide (DMSO) were purchased from Sigma Chemical Company (St. Louis, MO).

SDS-PAGE

Tris base, NuPAGE® Novex 10% Bis-Tris Gels, SeeBlue® Pre-Stained Standard, SimplyBlue™ SafeStain, NuPAGE® LDS Sample Buffer (4X), NuPAGE® Reducing Agent (10X), NuPAGE® Antioxidant, and MOPS Running Buffer were purchased from Invitrogen Life Technologies (Carlsbad, CA).

Restriction Digest

Restriction enzymes *Eco*RI, *Hind*III, and *Cla*I were purchased from New England Biolabs (Beverly, MA).

Plasmid DNA

The plasmid DNA YCp50 was a gift from Dr. Kevin Lewis. It was constructed as described by Campbell and Kuo (30).

Incubation of Plasmid DNA with KeAZB-037 and KeAZB-106

Compounds KeAZB-037 and KeAZB-106 were a gift from Dr. Sean Kerwin at the University of Texas at Austin.

Trypsin Digest

Acetonitrile, ammonium bicarbonate, dithiothreitol (DTT) and iodoacetamide were purchased from Sigma-Aldrich Company (St. Louis, MO). Trifloroacetic acid (TFA) was purchased from Pierce Biotechnology Inc. (Rockford, IL). Trypsin was purchased from Promega (Madison, WI).

Wavelength Scans

Bio-Rad SmartSpec™3000 Spectrophotometer (Hercules, CA) was used to determine absorbance spectra of aza-enediynes and incubated drug:protein samples.

Peptide Incubation

Bradykinin triacetate salt was purchased from Sigma-Aldrich Company (St. Louis, MO). Compounds KeAZB-037 and KeAZB-104 were a gift from Dr. Sean Kerwin at the University of Texas at Austin.

Biomolecular Interaction Analysis of p38α

Sensor chip CM5 (carboxymethylated dextran) , *N*-ethyl-*N*'-dimethylaminopropylcarbodiimide (EDC), *N*-hydroxysuccinimide (NHS), 1M ethanolamine (HCL, pH 8.5), and HBS-EP (0.01 M HEPES pH 7.4, 0.15 M NaCl, 3 mM EDTA, 0.005% v/v Surfactant P20) were purchased from BIACORE (Uppsala, Sweden). p38 was purchased from Sigma Chemical Company (St. Louis, MO). KeAZB-083, KeAZB-104A, and KeAZB-109A were a gift from Sean Kerwin at the University of

Texas at Austin. SB203580 was purchased from Calbiochem (La Jolla, CA). Experiments were performed on Biacore X SPR instrument (Uppsala, Sweden).

Molecular Modeling

Molecular modeling was carried out using commercially available Accelrys Cerius 2 software package (San Diego, CA).

II. METHODS

Sample Preparation

KeAZB-106 and KeAZB-037 were suspended in Tris buffer (10 mM, pH 7.0). BSA (0.6 mM) was incubated with KeAZB-106 (0.6 mM) at varying ratios of BSA: 106 (1:1, 1:4, and 1:10). BSA was incubated with KeAZB-037 (1.2 mM) varying ratios of BSA: 037 (1:1, 1:4, and 1:10). Two sets of each of the previous sample sets were prepared and incubated at 37 °C for 24 hours or at 70 °C for 30 minutes (high heat samples).

Restriction Digest

The plasmid DNA YCp50 was digested in three separate reaction mixtures with *Hind*III, *Eco*RI, and *Cla*I. In a 1.5 ml microfuge tube, the following were added: 2 µl YCp50 (760 ng/µl), 12.5 µl ddH_2O, 1.5 µl restriction enzyme, 4 µl 10X buffer, 6 µl TE buffer, 6 µl glycerol dye. The mixture was incubated at 37˚C for 2-4 hours. The samples were run on a 0.7% agarose gel, stained with ethidium bromide and visualized on a Kodak Image Station 440.

Incubation of Plasmid DNA with KeAZB-037 and KeAZB-106

The plasmid DNA YCp50 was incubated in two separate reaction mixtures with KeAZB-106, KeAZB-037. In a 1.5 ml microfuge tube, the following were added: 0.84 µl

YCp50 (760 ng/µl), 9 µl ddH_2O, 6.6 µl of KeAZB-106(200 µM), 2.6 DMSO, 1 µl Tris buffer. The other 1.5 ml microfuge tube contained the following: 0.84 µl YCp50 (760 ng/µl), 12.7 µl ddH_2O, 3.3 µl of KeAZB-037 (200 µM), 2.2 µl DMSO, 1 µl Tris buffer. The mixtures were incubated at 37 ˚C for 24 hours. Prior to loading, 4 µl of glycerol dye was added to all samples. The samples were run on a 0.7% agarose gel, stained with ethidium bromide and visualized on a Kodak Image Station 440.

Gel Optimization

Optimal conditions and amounts of BSA loaded onto 10% Bis-Tris gels were determined by preparing BSA: 106 samples at 1:4 (0.06 mM : 0.24 mM) and diluting the samples 1/6, 1/12, and 1/24. The samples were subjected to high heat at 70 ºC for 30 minutes prior to gel electrophoresis. The samples were prepared in 1.5 ml centrifuge tubes and contained 2.5 µl of the BSA: 106 samples, 2.5 µl of loading buffer, 1 µl of reducing agent and 4 µl of deionized water. The samples were heated for 10 minutes at 70 ºC prior to electrophoresis on a 10% Bis-Tris SDS-PAGE at 200V for 50 minutes in MOPS buffer pH 7.4.

SDS Page

The prepared samples were loaded on 10% Bis-Tris precast gels which were used as recommended by manufacturer instructions, except that gels were run for 100 minutes at 200V.

Spin Column Procedure

Micron YM-3 Centrifugal Filter Devices (Bedford, MA) were used to remove excess KeAZB-106 and KeAZB-037 from incubated BSA samples. The Micron YM-3 devices were composed of regenerated cellulose with a 3,000 molecular weight cutoff.

The incubated samples were placed into the Micron sample reservoir and centrifuged at 14,000 x g for 3 hours. The supernatant was discarded and the samples were rinsed with 10 µl acetonitrile at 14,000 x g for 15 minutes. The sample reservoir was removed and inverted onto a new vial and centrifuged at 1000 x g for 15 minutes after the addition of recovery buffer (15 µl of 10 mM Tris, pH 7).

Overloaded SDS-PAGE

An overloaded gel containing BSA: 106, 1:1 (0.06 mM : 0.06 mM), 1:4 (0.06 mM : 0.24 mM), and 1:10 (0.06 mM : 0.6mM) samples were run on 10% Bis-Tris SDS-PAGE at 200V for 100 minutes in MOPS buffer pH 7.4. The samples were subjected to high heat, 70 °C for 30 minutes prior to the spin column procedure. The samples were subjected to reducing versus nonreducing conditions for gel electrophoresis. The samples prepared under reducing conditions contained 6.5 µl of sample (BSA: 106), 1 µl of reducing agent, and 2.5 µl of loading buffer. The samples prepared under nonreducing conditions were prepared identically to the reduced samples, except that they contained 1 µl of water, which replaced the reducing agent.

In-Gel Trypsin Digest

BSA: 106 samples were subjected to high heat and the spin column procedures, then overloaded on a 10% Bis-Tris precast gel. The samples of interest were excised from the gel and cut to fine pieces. The gel slices were destained in 50% acetonitrile and 25 mM ammonium bicarbonate for 4 hours. The destain solution was removed and the sample was rinsed with 25 mM ammonium bicarbonate. Fifty microliters of 10 mM DTT in ammonium bicarbonate was added prior to incubation at 56° C for one hour. The DTT was removed and the sample was rinsed with 25 mM ammonium bicarbonate. Fifty

microliters of 55 mM iodoacetamide in 25mM ammonium bicarbonate was added and the sample was incubated at room temperature in the dark. The iodoacetamide was removed and the sample was rinsed several times for 10 minutes each time with ammonium bicarbonate. The sample was dried using a Savant Speedvac SC110 (Savant, NY). The sample was rehydrated in 25 mM ammonium bicarbonate. After the addition of five microliters of reconstituted trypsin (0.1 μg/μl), the sample was incubated overnight at 37 °C. The sample was periodically mixed for the first hour after the addition of trypsin. The supernatant was transferred to a new 1.5 ml centrifuge tube and the peptides were extracted with 50% acetonitrile containing 0.1% TFA. This step was repeated several times. The sample was then dried using the Savant Speedvac and reconstituted in 10% acetonitrile containing 0.1% TFA.

Peptide Mass Fingerprinting

Following the trypsin digest procedure, 1 μl of the trypsin digest sample was prepared for analysis using Zip-Tip (Millipore) reversed-phased cleanup and diluted 1:5 with α-cyano-4-hydroxcinnamic acid (CHCA) matrix solution. A 1 μl aliquot of the matrix solution was introduced to the MALDI target plate and the sample was allowed to air dry. Voyager-DE Pro mass spectrophotometer (Applied Biosystems, Framingham, MA) in reflector mode, with external calibration of the instrument over a 700-4000 *m/z* range was used to acquire spectra. An average of 2000 shots from a 337-nm nitrogen laser was applied. Samples for mass fingerprinting were analyzed by Dr. Maria Person at the University of Texas at Austin.

Sample Preparation for Wavelength Scans

Incubated samples (BSA: 106 and BSA: 037) were subjected to Micron YM-3 Centrifugal Filter Devices (Bedford, MA) in order to remove excess KeAZB-106 and KeAZB-037. The Micron YM-3 devices were composed of regenerated cellulose with a 3,000 molecular weight cutoff. The incubated samples were placed into the Micron sample reservoir and centrifuged at 14,000 x g for 3 hours. The supernatant was discarded and the samples were rinsed with 10 µl acetonitrile at 14,000 x g for 15 minutes. The sample reservoir was removed and inverted onto a new vial and centrifuged at 1000 x g for 15 minutes after the addition of recovery buffer (15 µl of 10 mM Tris, pH 7). The samples were scanned from 200-600 nm using SmartSpec-100. The instrument was blanked with Tris buffer. Samples were 0.06 mM each.

Peptide Incubation Procedure

Bradykinin (1 mM) was incubated with KeAZB-104 and KeAZB-037 at 70 °C for 24 hours. The control sample contained 250 µM bradykinin in Tris buffer (10 mM, pH 7.0) with 2.5 % DMSO. The incubated samples contained a 1:1 ratio of bradykinin to either KeAZB-104 or KeAZB-037, both in the same buffer as the control sample.

Peptide MALDI Analysis

Aliquots of the bradykinin incubated samples were analyzed by MALDI at the University of Texas at Austin by Dr. Maria Person. The samples were prepared for analysis using Zip-Tip (Millipore) reversed-phased cleanup. The same procedure was followed as for Peptide Mass Fingerprinting above, except an average of 3000 shots from a 337-nm nitrogen laser was applied.

The Immobilization of Unphosphorylated p38α

A preconditioned CM5 sensor chip was docked into the Biacore X. Two consecutive washes (50 µl) of each solution with 50mM NaOH and 1M HCl, 10mM HCl and 1% SDS, and finally water were performed at a flow rate of 100 µl/min. Standard amine coupling procedures were performed to prepare the surface of p38α. SB-203580 (10 µM) was present at a saturating concentration to stabilize p38α during the coupling procedure. A 10µl/min flow rate of HBS-EP was used for immobilizations which were carried out at 25 °C. A 70 µl mixture of 50 mM NHS: 200 mM EDC was injected for 7 minutes to activate the flow cells. This was followed by an injection of a mixture which contained 50 µl of p38α (50 µg/ml) mixed with 10 µM SB-203580 in sodium acetate, pH 5.5. The injection lasted 5 minutes and was followed by 35 µl of ethanolamine. The ethanolamine solution served to block any remaining activated ester groups.

Binding Analysis

In each case, the chip containing immobilized p38 was equilibrated by injections of running buffer (HBS-EP) prior to any binding analysis. Injections of SB-203580 (3 µM) were performed at 10 µl/min for 10 minutes with a delay wash of 180 seconds. KeAZB-083 and KeAZB-104 were both injected at a concentration of 10 µM. Injections of KeAZB-083 were typically at a flow rate of 5 µl/min with a delay wash of 180 seconds, while injections of KeAZB-104 were performed at 5, 10, and 20 µl/min with a 120 second delay wash.

Molecular Modeling

The COMPASS forcefield reported by Sun and Ren (31) and Sun (32) was used for all calculations. Compounds KeAZB-037, KeAZB-083, KeAZB-104, KeAZB-106,

KeAZB-109, and SB-203580 were built using 3D Sketcher, and charges were calculated using the open force field setup module (33, 34). A series of minimization and dynamics was performed to produce the most stable configuration. A crystallographic model of p38 docked with inhibitor molecule 3- (benzyloxy) pyridine-2-amine was imported as a .pdb file from the RCSB Protein Data Bank into Cerius 2 software. The imported model did not contain hydrogen residues. Hydrogen atoms were added using 3D Sketcher to the residues near the p38 active site including (benzyloxy) pyridine-2-amine. Since p38 is a large molecule, atom positions of all molecules outside of the active site pocket were constrained using the minimizer, fix atom position function. Charges for non-constrained residues were calculated. A series of minimizations and molecular dynamics were carried out while undefined terms were ignored in the calculations using the open force field set up. The energy of p38 active site pocket docked with (benzyloxy) pyridine-2-amine was calculated and compared to the energy of p38 alone. The energy difference was used to determine the strength of the non-covalent interactions between the protein and the inhibitor molecule. The bond lengths were calculated using the Geometry Measurement function. Hydrogen bonds were defined using the Hydrogen Bond Editor function. The bonds lengths for residues His 107 and Met 109 were compared to values reported by Hartshorn *et al.* (28). Compounds KeAZB-037, KeAZB-083, KeAZB-104, KeAZB-106, KeAZB-109, and SB-203580 were loaded from 3D Sketcher then docked into the active site of p38, replacing (benzyloxy) pyridine-2-amine. The steps described above were repeated to compare the strengths of interactions of (benzyloxy) pyridine-2-amine, KeAZB-037, KeAZB-083, KeAZB-104, KeAZB-106, KeAZB-109, and SB-203580.

CHAPTER 3

RESULTS AND DISCUSSION

Although aza-enediynes form reactive intermediates which may participate in DNA cleavage (14-16), the interaction of aza-enediynes with proteins has not been studied. The primary goal of this research was to investigate potential interactions between imidazole and pyridine-based aza-enediynes with proteins (Chapter 1, Figure 6). Initially, the ability of KeAZB-106 and KeAZB-037 to modify a model protein, BSA, was determined. Several experiments yielded results which led us to investigate interactions between additional representative aza-enediynes and p38. The series of KeAZB compounds resemble known inhibitors of p38, so binding analysis using Biacore's Surface Plasmon Resonance phenomenon was conducted to determine the affinity of the protein for the compounds under investigation. Modeling studies of p38 with KeAZB-106, KeAZB-104, KeAZB-109, KeAZB-083, KeAZB-037, and SB203580 were done in order to provide a 3D representation of the proposed interactions, and to evaluate the proposed inhibitors compared to a small inhibitor molecule, (benzyloxy) pyridine-2-amine reported by Hartshorn *et al.* (28). To evaluate the ability of KeAZB-106 and KeAZB-037 to cleave DNA, a gel electrophoresis experiment was performed. The confirmation of the ability of KeAZB-106 and KeAZB-037 to cleave DNA provided reassuring evidence that the molecules were active. The DNA plasmid chosen was YCp50 (30), (Figure 7).

DNA Cleavage Ability of Aza-Enediynes

YCp50 is a supercoiled DNA plasmid which contains a single *Eco*RI, *Hind*III, and *Cla*I restriction site. *Eco*RI, *Hind*III, and *Cla*I were used as positive controls for cleavage of YCp50. Aza-enediynes KeAZB-106, KeAZB-037, or KeAZB-037N were incubated with YCp50 at 37 °C for 24 hours. The samples containing YCp50 and restriction enzymes *Eco*RI, *Hind*III, and *Cla*I were incubated at 37 °C for 2 hours. All samples were loaded onto a 0.7% agarose gel and run at 100V for 100 minutes. Following staining with ethidium bromide, the gel was visualized on a Kodak Image Station 440.

The cleavage using restriction fragments was compared to cleavage of YCp50 using KeAZB-106 and KeAZB-037 (Figure 8). The results indicate restriction enzymes *Eco*RI and *Cla*I cleave at one restriction site yielding one band, indicating linearized plasmid (Figure 8, lanes 7 and 8, respectively). *Hind*III was expected to produce the same type of result but instead yielded two bands, indicating incomplete linearization (Figure 8, lane 6). Control samples of YCp50 incubated in the absence of drug or restriction enzyme exhibit very little cleavage compared to samples of plasmid DNA incubated with drug (Figure 8, lanes 1 and 5 compared to lanes 2-4). Significant amounts of circular plasmid DNA are observed after incubation of the plasmid with KeAZB-106, KeAZB-037, and KeAZB-037N. KeAZB-037N is the same compound as KeAZB-037, but was a freshly prepared stock. It is probable to conclude that the compounds lose reactivity over time.

After noting that compounds KeAZB-106, KeAZB-037, and KeAZB-037N have the ability to cleave plasmid DNA YCp50, experiments were performed to determine whether these compounds interact with proteins or a peptide (bradykinin).

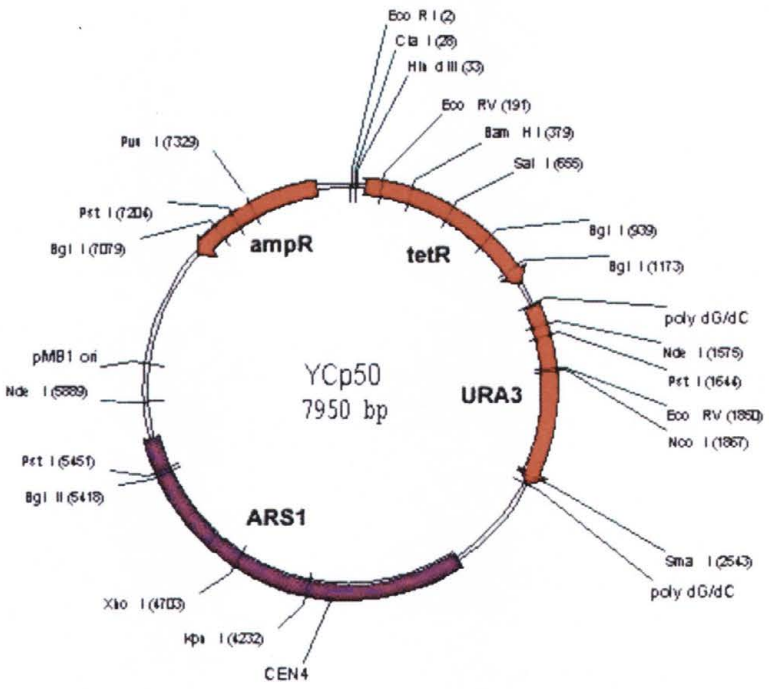

Figure 7. Plasmid DNA YCp50.

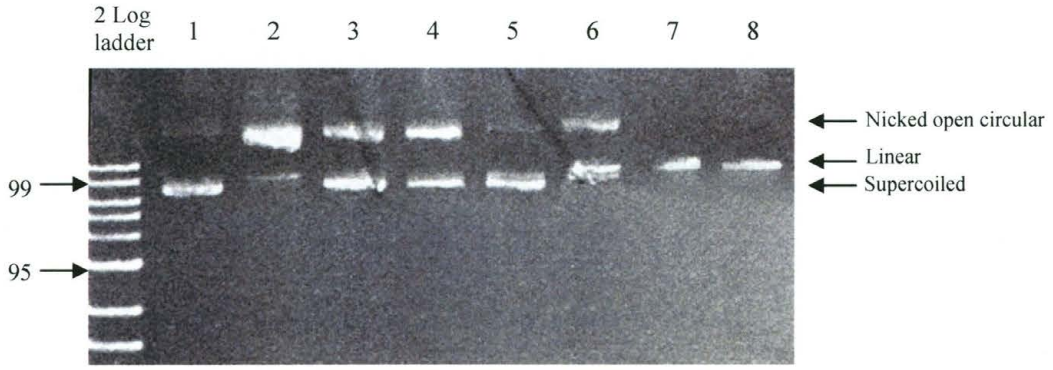

Figure 8. DNA cleavage ability of aza-enediynes. The control lanes (1 and 5) consist of DNA plasmid YCp50. Lanes 2, 3, and 4 contain YCp50 incubated with KeAZB-037N, KeAZB-037, and KeAZB-106, respectively. Lanes 6, 7, and 8 are the restriction products obtained from incubation of YCp50 with *Hind*III, *Eco*RI, and *Cla*I.

Optimization of SDS-PAGE Conditions for Monitoring Interaction Between Aza-Enediynes and BSA

BSA was chosen as a model protein for the following experiments because it is well characterized and readily available. If incubation of BSA with aza-enediynes were to result in protein cleavage or extensive covalent modification, a gel shift may result. Gel conditions for SDS-PAGE were optimized (Figure 9).

The samples used for this experiment were BSA: 106 (1:4, 0.06 mM: 0.24 mM). The samples were heated for 10 minutes at 70 °C prior to analysis by 10% Bis-Tris SDS-PAGE at 200V for 50 minutes in MOPS buffer (pH 7.4).

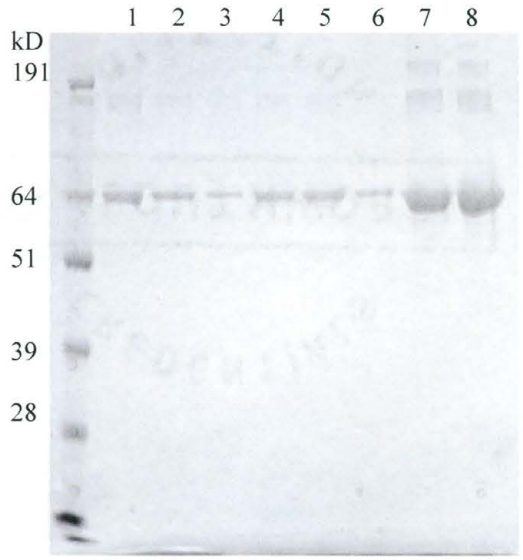

Figure 9. Optimal conditions for BSA analysis. Lanes 1-3 contain BSA only and serve as control lanes at 1/6 (1600 ng BSA), 1/12 (800 ng BSA), and 1/24 (400 ng BSA) dilutions of stock solutions. Lanes 4-6 correspond to the incubated samples of BSA:106 (1:4), and are dilutions of 1/6, 1/12, and 1/24 respectively. Lanes 7 and 8 are samples which have not been diluted. Lane 7 is BSA alone and lane 8 is BSA: 106 (1: 4).

The gel electrophoresis results indicate that the 1/24 dilution containing 400 ng of BSA produced the sharpest bands, a necessary condition for visualizing possible modifications such as protein cleavage or covalent adducts that may occur between BSA and KeAZB-106.

Gel Shift Assays for Monitoring Interaction Between Aza-Enediynes and BSA

After the optimal gel conditions had been studied, samples were prepared at BSA: 106 and BSA: 037 ratios of 1:1, 1:4, and 1:10. Duplicate sets of samples were prepared under incubation conditions at 37 °C for 24 hours or 70 °C for 30 minutes. Slight gel

shifts were observed in the BSA: 106 samples which were incubated at 70 °C for 30 minutes and in the BSA: 106 samples which were incubated at 37 °C for 24 hours (Figure 10 and 11, respectively); however it is unclear whether the gel shifts are due to inconsistent band intensity among each lane. Gels shown in Figure 10 and Figure 11 were run under reducing *versus* nonreducing conditions using 10% Bis-Tris SDS-PAGE gels at 200V for 100 minutes in MOPS buffer (pH 7.4).

In order to rule out slight gel shifts possibly resulting from gel oxidation or modification of the free cysteine thiol groups in BSA, reducing *versus* nonreducing conditions were compared. Reducing conditions generated the sharpest and best behaved gel bands, but the overall trend in migration appears the same regardless of the presence or absence of reducing agent.

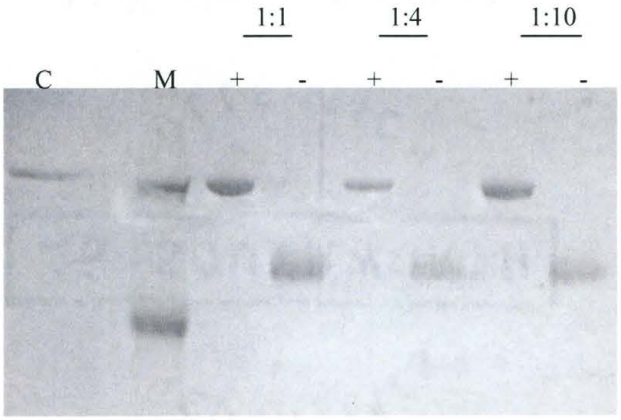

Figure 10. BSA samples subjected to high heat. The samples (C= control which contains only BSA, 1:1 BSA: 106, 1:4 BSA:106, and 1:10 BSA:106) were subjected to high heat at 70 °C for 30 minutes prior to electrophoresis. Protein molecular weight standard, M, contains two bands (64 and 51 kDa). The absence and presence of reducing agent are represented by (-) and (+) respectively.

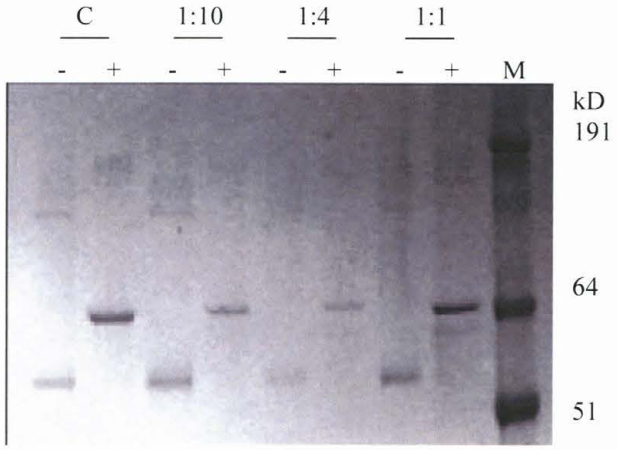

Figure 11. BSA 37 °C incubated samples. The samples (C = control which contains only BSA , 1:1 BSA: 106, 1:4 BSA:106, and 1:10 BSA:106) were incubated at 37 °C for 24 hours prior to electrophoresis. The absence and presence of reducing agent are represented by - and + respectively.

In order to determine if the slight observed shifts were an artifact occurring due to excess drug in the gel samples, a new set of samples was prepared and subjected to a 3,000 molecular weight cutoff spin column in order to remove excess unreacted KeAZB-106. Since BSA has a molecular weight of approximately 64 kD and KeAZB-106 has a molecular weight of 160 g/mol, any unadducted KeAZB-106 would flow through the cellulose column and be discarded.

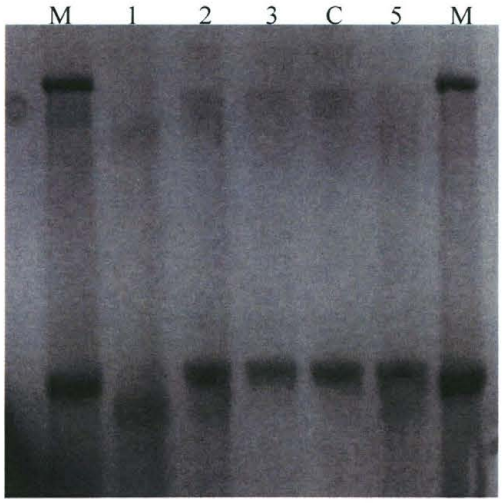

Figure 12. High heat spin column samples. Lane 1, 2, and 3 correspond to BSA: 106, 1:10, 1:4, and 1:1 samples. Lane 4 is the control sample which contains only BSA and lane 5 is a sample which was not subjected to the spin column procedure. Protein molecular weight standard, M, contains two bands (191 and 64 kDa).

A set of samples of BSA: 106 was prepared and subjected to high heat, 70 °C for 30 minutes. Excess KeAZB-106 was removed using Micron YM-3 Centrifugal Filter Devices. The sample was recovered in 20 µl of Tris buffer (10mm, pH 7.0). The recovered samples were analyzed by 10% Bis-Tris SDS-PAGE at 200V for 2.75 hours in MOPS buffer (pH 7.4) (Figure 12). After exposure to high heat, a lower molecular weight fragment was observed for the 1:10 (BSA: 106) sample, (Figure 12, lane 1), possibly indicating cleavage of a small segment of BSA :106 protein complex. This does not rule out the possibility of sample contamination.

An overloaded gel containing BSA:106 samples which were exposed to high heat and Micron YM-3 spin columns was performed under the same conditions as used

previously. Three samples (control, 1:4, and 1:10) were excised and digested with trypsin as described in the Methods section. The resulting tryptic peptides were analyzed by matrix assisted laser desorption ionization – time of flight mass spectrometry (MALDI-TOF) in order to identify a modified BSA fragment.

The results indicate that the control sample which contained BSA alone was no different than the incubated BSA: 106 samples (Figure 13). Observed peptide fragments from trypsin digestion of BSA are listed in Table 1. No additional modified peptides are observed in samples resulting from incubation of BSA with KeAZB-106. Since the size of BSA relative to KeAZB-106 is large, it may be difficult to monitor an adduct or modification. The samples were stored at -80 °C prior to analysis by MALDI-TOF to minimize any degradation of a potential adduct. If an interaction between BSA and KeAZB-106 occurred, it is possible that the interaction was unstable and not observed.

These results led to an experiment where bradykinin was incubated with compounds KeAZB-106 and KeAZB-037. Since the size of bradykinin (1240.36 g/mol) is drastically smaller than BSA (64 kDa), and trypsin digestion is unnecessary, it is conceivable to predict that an interaction may be more readily monitored by MALDI-TOF mass spectrometry.

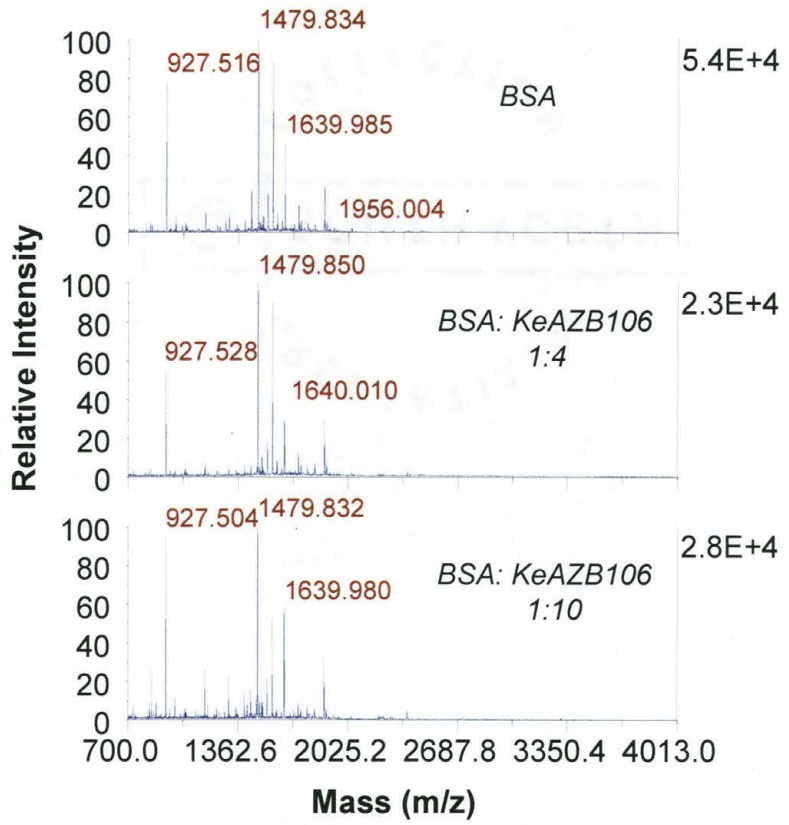

Figure 13. MALDI-TOF mass spectra of BSA tryptic digests. The digests were diluted 1:5 in cyano-4-hydroxycinnamic acid and analyzed as described in the Methods section. Table 1 lists the corresponding peptide sequences and expected m/z[a].

Table 1 BSA tryptic peptides identified by MALDI-TOF-MS.

Peptide *m/z* [a]	Calculated *m/z* [a]	Peptide sequence identified	Sequence start-end
927.516	927.4940	(K)YLYEIA(R)	161-167
1439.840	1439.8123	(R)RHPEYAVSVLLR(L)	360-371
1479.834	1479.7960	(K)LGEYGFQNALIVR(Y)	421-433
1639.985	1639.9383	(R)KVPQVSTPTLVEVSR(S)	437-451
1956.004	1955.9602	(K)DAIPENLPPLTADFAEDK(I)	319-336

[a] Monoisotopic *m/z*

Wavelength Scan Data

Wavelengh scans from 200 nm to 600 nm were performed on incubated samples of BSA: KeAZB-106, and BSA: KeAZB-037 at varying ratios (1:1, 1:4, and 1:10). The incubated samples were subjected to spin columns with a 3,000 molecular weight cut-off to remove any unbound drug. The BSA control sample produced a maximum absorbance in the 220-280 nm range (Figure 14A). Incubated BSA:106 samples had maximal absorbance in the same range (Figure 14D). Differences were not observed, however a true difference spectrum needs to be obtained in order to calculate differences. In contrast, the incubated BSA:037 (1:10) sample had maximal absorbance at 260-280 nm, and a second maximum at about 360-400 nm (Figure 14C). The sample was compared to KeAZB-037 sample which was not incubated, and KeAZB-037 also absorbs in the region 360-400 nm (Figure 14B). Since the incubated BSA:037 sample absorbs in the same range as KeAZB-037 alone, it is probable that an interaction between the molecules occurred. KeAZB-037 has a molecular weight of 416.66 g/mol if unreacted, therefore, it is expected to flow through the spin column.

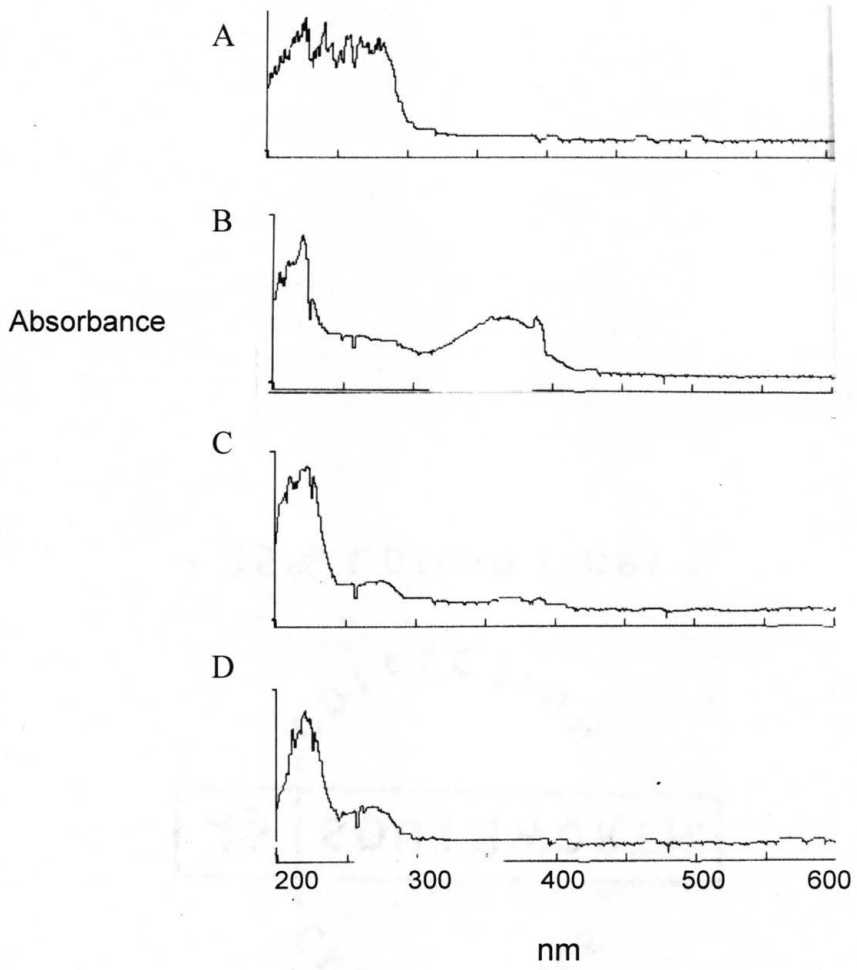

Figure 14. UV absorption spectra of BSA/drug samples. A) Sample containing BSA alone (Tris 10 mM pH 7.0) produced a maximum absorbance in the 220-280 nm range. B) Compound KeAZB-037 in Tris buffer. C) BSA:037 (1:10) incubated sample. D) BSA:106 (1:4) incubated sample.

Bradykinin Incubation with KeAZB-037 and KeAZB-104

KeAZB-104 and KeAZB-037 were incubated with bradykinin at 70 °C for 24 hours. A control sample contained bradykinin in the absence of aza-enediynes. The samples were analyzed by MALDI-TOF mass spectrometry in order to determine if the peptide was modified. The results suggest that compound KeAZB-104 (Figure 15B) modified bradykinin. A new peak at 1282.65 m/z is equal to the mass of the bradykinin peptide (1060.56 daltons) and KeAZB-104, which has a mass of 222.11 daltons. The mass spectrum corresponding to bradykinin incubated with compound KeAZB-037 (397.06 daltons) also contains a new peak, indicating that the peptide was modified covalently (Figure 15C). However, the mass change does not correspond to a simple addition of KeAZB-037 and further analysis is required to identify the modification. To further characterize the type of interaction in both cases, tandem mass spectrometry needs to be performed. After studying the interactions of aza-enediynes with bradykinin, a predicted interaction between p38α and aza-enediynes was measured using surface plasmon resonance.

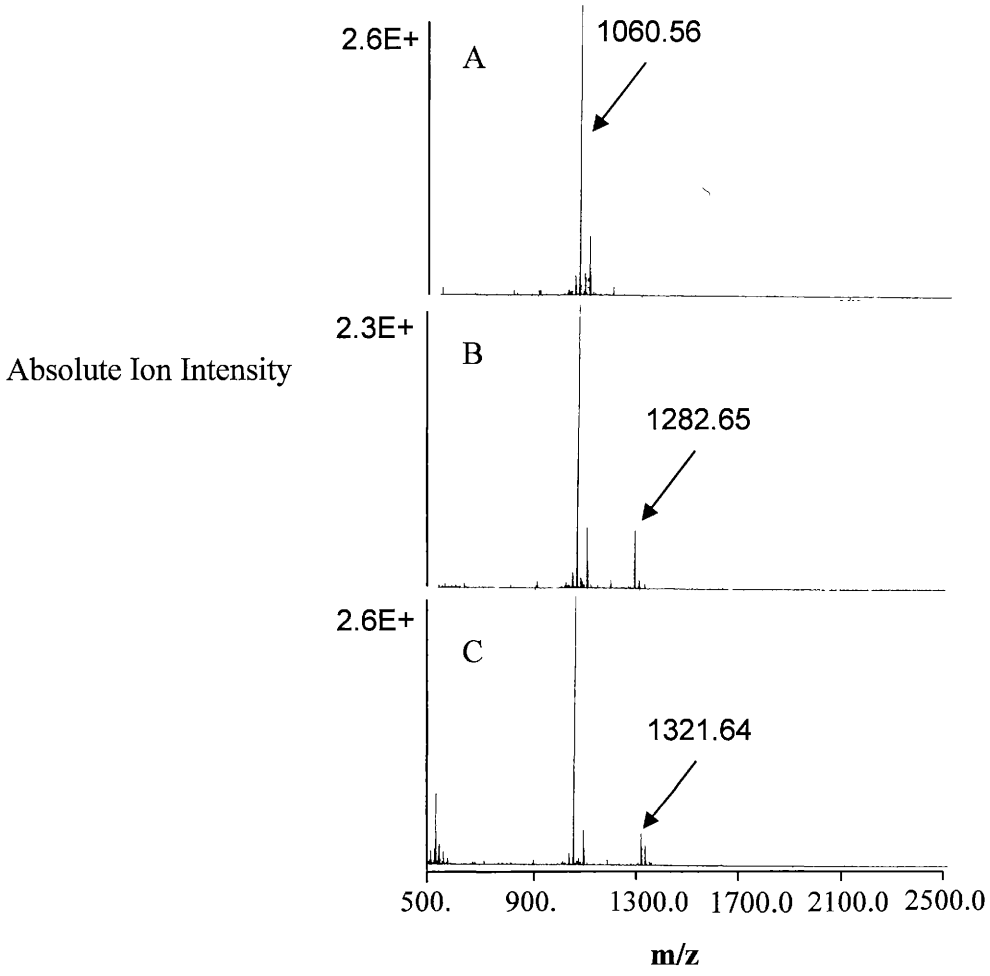

Figure 15. MALDI-TOF analysis of bradykinin with aza-enediynes. (A) Bradykinin control incubated at 70 °C for 24 hours. (B) KeAZB-104 incubated with bradykinin under the same conditions. (C) KeAZB-037 incubated with bradykinin under the same conditions.

Biacore Binding Studies of Aza-Enediynes and p38α

Inactive p38α was immobilized on a CM5 sensor ship in the presence of SB-203580, a reversible inhibitor. The dextran matrix on the sensor surface was activated with a mixture of EDC and NHS, via standard amine coupling procedures. This produced activated succinimide esters on the surface of the chip, to which amino groups or nucleophilic groups on the ligand (p38) were covalently linked (Figure 16). Remaining active esters were then deactivated (capped) with ethanolamine. The immobilization rate was 10 μl/min. The resonance responses observed during the steps involved in the immobilization procedure are shown in Figure 17. The addition of SB-203580 to p38 is known to stabilize p38 on the sensor surface of Biacore chips. Casper *et al.* reported a low activity (15%) biosensor surface in the absence of SB-203580 and a significant increase in surface activity (90 %) when p38 is ligand-stabilized with SB-203580 (25). The immobilization was performed at a pH of 5.5, where SB-203580 induces structural stabilization of p38 (25). After immobilization, SB-203580 is easily removed during wash procedures. Prior to the binding analysis p38 must be immobilized on the sensor surface at sufficient levels in order to observe a response from the binding of a small molecule analyte. A response in resonance was measured after the ligand-stabilized p38 was introduced. The RU response measured was 4862. This value is comparable to surface density of 3000-5000 RU reported by Casper *et al.* (25).

Compounds SB-203580, KeAZB-083, KeAZB-104, and KeAZB109 were passed over the sensor surface to determine whether or not binding was exhibited. Sensorgrams shown in Figures 18-19 are corrected for nonspecific binding to an unmodified dextran surface using a reference cell. SB-203580 was injected at 10 μl/min flow rate for 10

minutes at a concentration of 3 μM with a delay wash of 180 seconds. The association is shown by the increase in response, while the dissociation is shown by a decrease in response (Figure 18). The response observed was 18.4 RU, comparable to a response of ~ 30 RU reported by Casper *et al.* (25). The maximum theoretical binding of an analyte to a derivatized chip, R_{max} , can be calculated according to equation 1, where MW_A/MW_L is the ratio of molecular weight of analyte to ligand, R_L is the amount of ligand bound to the sensor surface in RU, and S_m represents the stoichiometry of analyte to ligand. The S_m value can account for multiple binding sites. Since we expect a 1:1 ratio in the experiments described, S_m equals 1. In this case, the MW_A/MW_L ratio is 0.00993, and R_L 4862 RU. Thus, the R_{max} of 48.28 RU was calculated.

$$R_{max} = MW_A/MW_L\,(R_L)(S_m) \qquad \text{Equation 1}$$

Compounds KeAZB-083, KeAZB-104, and KeAZB-109 were injected at a concentration of 10 μM. One hundred microliters of KeAZB-104 were injected at 20 μl/min with a 120s delay wash (Figure 19). The response observed for KeAZB-104 was 4.2 RU. For KeAZB-104, the MW_A/MW_L ratio is 0.00584, thus an R_{max} of 28.43 RU was calculated. KeAZB-104 exhibited minimal binding, where the binding was slow and the interaction was weak. Compound KeAZB-083 did not bind to p38 (Figure 20) at a flow rate of 5 μl/min with a 180 second delay wash. KeAZB-083 has a MW_A/MW_L ratio of 0.00824, and R_{max} of 40.07 RU. The RU value for KeAZB-083 observed was -0.9. KeAZB-109 produced a response similar to KeAZB-083, where no binding was exhibited.

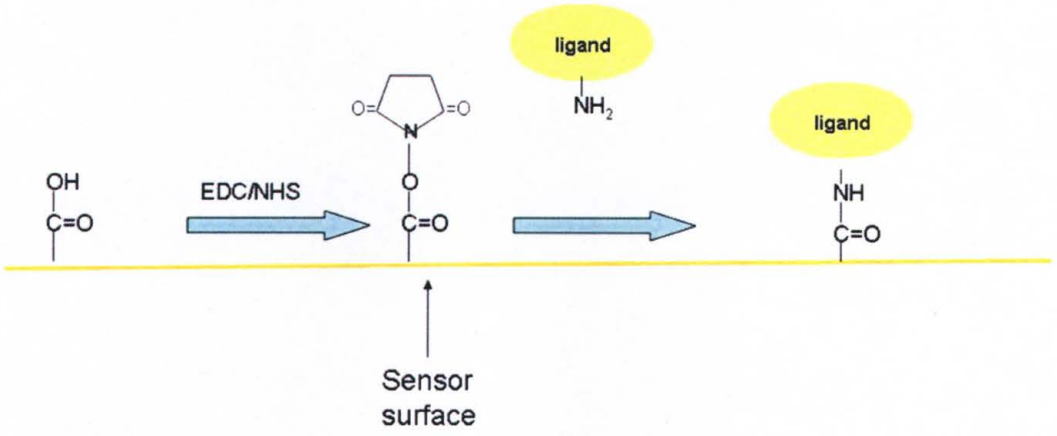

Figure 16. Amine coupling of ligand to sensor surface.

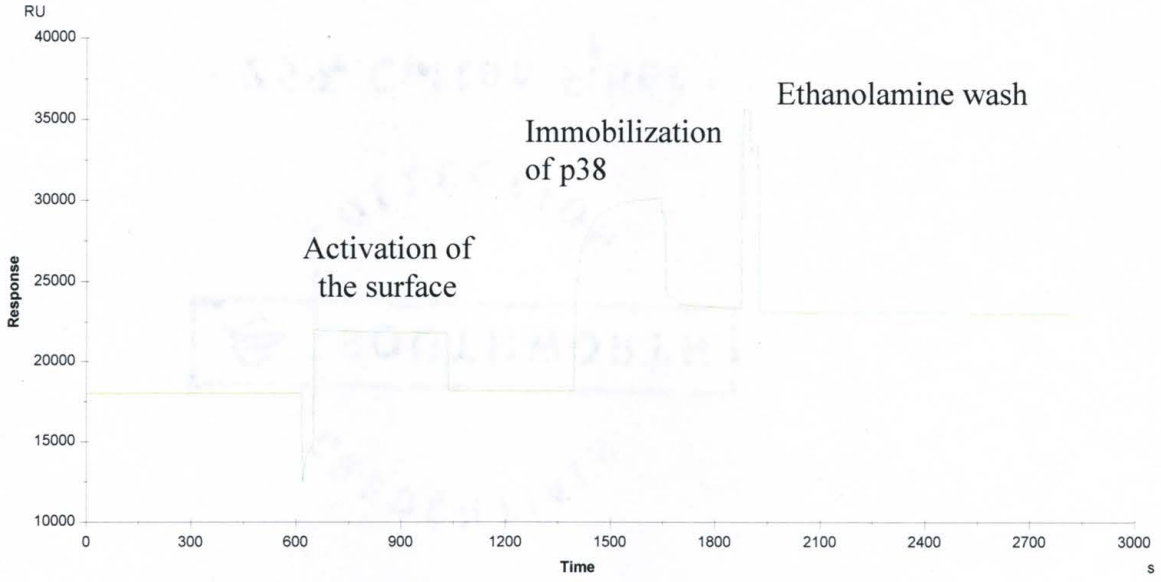

Figure 17. Immobilization of p38 onto carboxymethylated dextran surface.

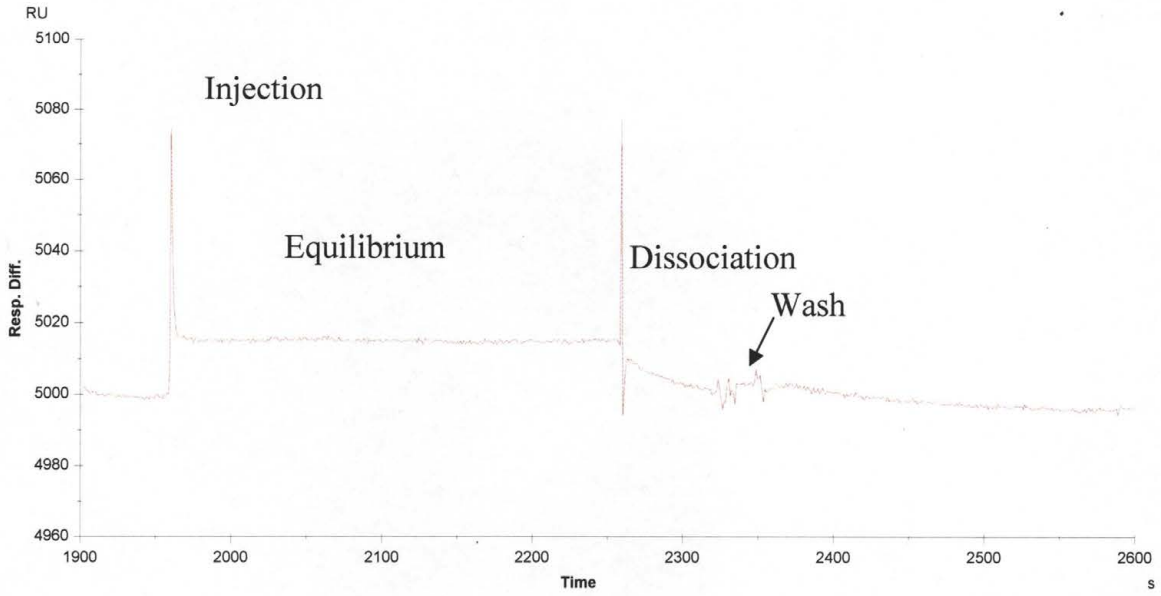

Figure 18. Binding of SB-203580 to p38 immobilized on the sensor surface.

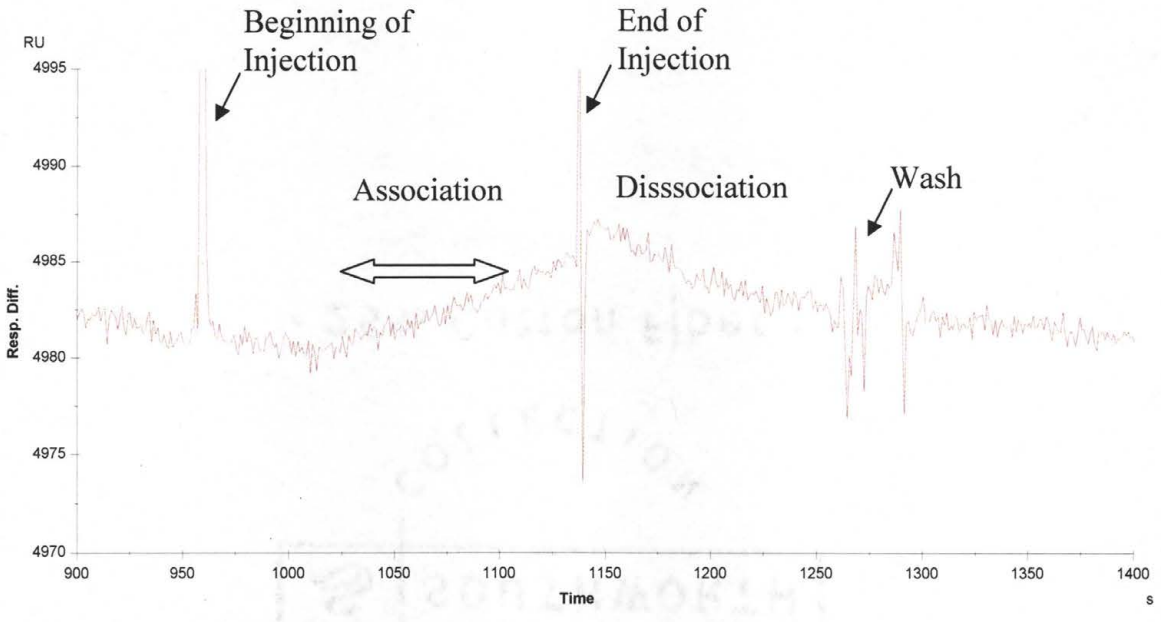

Figure 19. Binding of KeAZB-104 to p38 on carboxymethylated dextran surface.

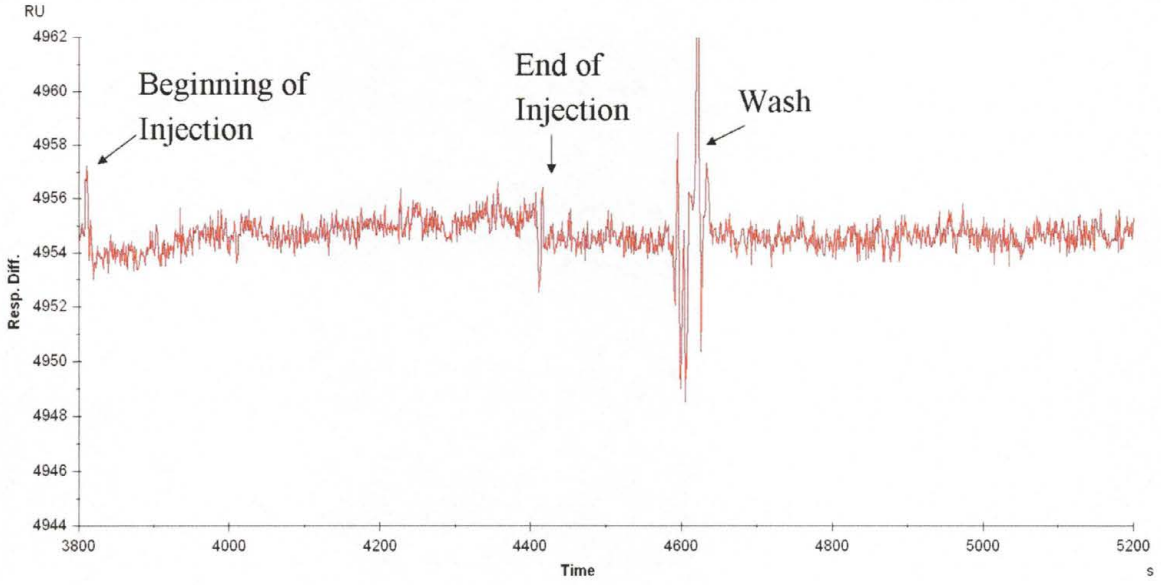

Figure 20. KeAZB-083 injections onto immobilized p38; no binding is exhibited.

Molecular Modeling of p38 Interactions with Aza-Enediynes

In comparing the structures of known inhibitors SB-203580 and RWJ 67657, it is important to note that pyridyl and *p*-fluorophenyl substituents of RWJ 67657 and SB-203580 are absent from aza-enediynes. However, KeAZB-037 and KeAZB-104 provided substantial stability to the active site of p38 during modeling simulations. When comparing these structures, the first similarity noted is that they are planar and do not occupy a large 3D sphere. In 3D space these compounds seem to be elongated along the active site of p38. Secondly, both structures possess an alkynyl-substituted ring similar to the known inhibitors. In contrast, KeAZB-109 and KeAZB-083 are bulky and rather than providing stability to the pocket, they introduce steric strain.

Molecular modeling studies were performed using Cerius 2 software package to determine which residues in the active site may stabilize the interaction of p38 MAP kinase with aza-enediynes KeAZB-037, KeAZB-083, KeAZB-104, KeAZB-106, and KeAZB109. The active site residues were determined based on a model of p38 with a small inhibitor molecule, 3- (benzyloxy) pyridine-2-amine which was imported from the Protein Data Bank. Hartshorn *et al.*, report that Met 109 and His 107 are involved in hydrogen bonding to the inhibitor molecule (28). The imported model was constructed based on crystallographic data. After the model was imported, slight modifications were made. Hydrogens not present in the model were added to give a better estimation of hydrogen bonding interactions. Energy calculations were performed to determine which inhibitor provided greatest stability in the active site.

A representation of p38 with KeAZB-106 in the active site is shown in Figure 21. Figure 22 is a close-up view of KeAZB-106 in the active site. The molecule has a total energy of -650.794 kcal/mol. In order to measure the interaction in the active site, KeAZB-106 was removed and the total energy was re-calculated. The energy difference calculated is 6.398 kcal/mol, which suggests that this compound contributes minimally to the overall stability of the active site. One hydrogen bond in the active site, with a length of 2.41Å may be present (Figure 22). A free carboxyl group on Asp 168 is shown interacting with the terminal yne portion of KeAZB-106. It is likely that hydrophobic residues, such as Tyr 35, Ala 51, Met 109, Leu 75, and Lys 53, which are present in the active site pocket, provide stability.

In contrast, the calculated values for binding of KeAZB-037 and 3- (benzyloxy) pyridine-2-amine are -652.496 kcal/mol and -571.035 kcal/mol respectively. When

KeAZB-037 is removed the active site pocket energy value is -625.037 kcal/mol, a total energy difference of 27.459 kcal/mol. When 3- (benzyloxy) pyridine-2-amine is removed from the active site pocket the energy value is -546.01 kcal/mol, giving a total energy difference of 25.11 kcal/mol. The destabilization of the active site upon removal of drug from the active site can be attributed to the removal of hydrogen bonds between drug molecules and active site residues which stabilize the active site pocket, as well as hydrophobic interactions that arise from the aromatic structures of KeAZB-037 and 3-(benzyloxy) pyridine-2-amine. For example, the terminal methoxyphenyl group of KeAZB-037 is stabilized by stacking interactions with the aromatic ring of Tyr 35. (Figure 23). Additionally, the nitrogen contained on the opposite ring portion of KeAZB-037 forms a hydrogen bond (1.98Å) with Tyr 106. Hydrophobic residues such as Val 52, Val 105, Leu 104, Leu 108, Ala 51 and Lys 53 provide further stability (not shown for clarity, Figure 23).

3- (Benzyloxy) pyridine-2-amine forms hydrogen bonds with Met 109 and His 107; the bond lengths obtained from the modeling experiment were 2.16Å and 2.67Å respectively (Figure 24). The values are similar to the literature values presented by Hartshorn et al. which are 2.94Å for Met 109 and 2.62Å for His 107. Tyr 35 forms stacking interactions with the ring containing a nitrogen in 3- (benzyloxy) pyridine-2-amine (Figure 24). Amino acid residues Lys 53 Leu 75, and Leu 104 contribute to hydrophobicity of the active site pocket.

The following compounds were modeled in the active site of site of p38 in order to provide comparative data for the experiments performed using Biacore X for biomolecular interaction analysis. Compounds KeAZB-083, KeAZB-104, and KeAZB-

109 were expected to bind the active site of p38 since they resemble known inhibitors. The energy values obtained from the modeling iterations are listed in Table 2. A negative energy difference corresponds to molecules which stabilized the active site of p38, whereas a positive energy difference indicates that the drug destabilizes the active site pocket.

KeAZB-083 is comprised of an imidazole ring and two aromatic rings. This molecule introduces steric hindrance to the active site pocket. Therefore, the energy of the active site pocket was calculated at -422.839 kcal/mol in the presence of KeAZB-083 and -574.885 kcal/mol in the absence, an energy difference of 152.406 kcal/mol. This is consistent with the biomolecular interaction studies, where KeAZB-083 does not bind to p38. KeAZB-109 produced similar molecular modeling data. The total energy of the active site in the presence of KeAZB-109 is -563.646 kcal/mol, lower by 28.15 kcal/mol in the absence (-591.799 kcal/mol) of the compound. A hydrogen bond (1.83 Å) from a methoxy group to Lys 53 was present (Figure 26). This is consistent with the biomolecular interaction analysis because KeAZB-109 did not bind to p38. In contrast to the bulky compounds KeAZB-083 and KeAZB-109, compound KeAZB-104 stabilized the active site of p38. The calculated energy value for this compound is -678.253kcal/mol. When the compound is removed from the active site pocket the calculated energy value is -631.211 kcal/mol. The 47.042 kcal/mol difference can be attributed to stability of stacking interactions caused by Tyr 35 and the aromatic portion of KeAZB-104 and hydrophobic residues Leu 75, Leu 108, Ala 51 and Val 52 present in the active site pocket (Figure 27). These data are consistent with Biacore studies which showed that KeAZB-104 binds the active site of p38.

Pyridinyl compound SB-203580 has been reported to inhibit p38 activity by Han *et al.* and Cuenda *et al.* (35, 36). SB-203580 is a reversible inhibitor of p38. SB-203580 stabilizes the active site of p38, allowing increased binding of the correct conformation of p38 to the Biacore sensor suface. The molecular modeling data indicate that the compound does not stabilize the active site of p38. The calculated energy of the molecule in the presence of SB-203580 is 0.614 kcal/mol and -229.96 kcal/mol in the absence. These data are inconsistent with Biacore studies where SB-203580 stabilized p38 on the sensor surface and also bound reversibly to the protein.

Although SB-203580 hydrogen bonds to residues in the active site (Figure 28), the molecule is located in the outer portion of the pocket of p38. This is caused by the dynamic simulation which configures the molecule in the most stable form (which in this case is furthest away). A similar trend was observed for molecules which were bulky. They did not stabilize the active site pocket. This occurred due to the constraints set on p38 amino acid residues which were not in the active site. The modeling program was unable to calculate how the entire protein might reconfigure in the presence of an inhibitor due to these constraints. This modeling program does not account for the reconfiguration that occurs according to the induced fit model of binding between a protein active site and substrate. In addition, the hydrogen bonds and stacking interactions between the compounds under investigation and p38 do not account for any hydrogen atoms which come from water molecules in the active site. Future studies include modeling the bulky compounds in the absence of constraints.

Table 2 Calculated energy values obtained from Molecular Modeling.

Compounds	Total Energy (kcal/mol)	Total Energy in absence of compound (kcal/mol)	Energy Difference (kcal/mol)
KeAZB-037	-652.496	-625.037	-27.459
KeAZB-083	-422.839	-574.885	152.046
KeAZB-104	-678.253	-631.211	-47.042
KeAZB-106	-650.794	-644.396	-6.398
KeAZB-109	-563.646	-591.799	28.15
SB-203580	.614	-229.96	229.346
3-(benzyloxy) pyridine-2-amine	-571.035	-546.01	-25.11

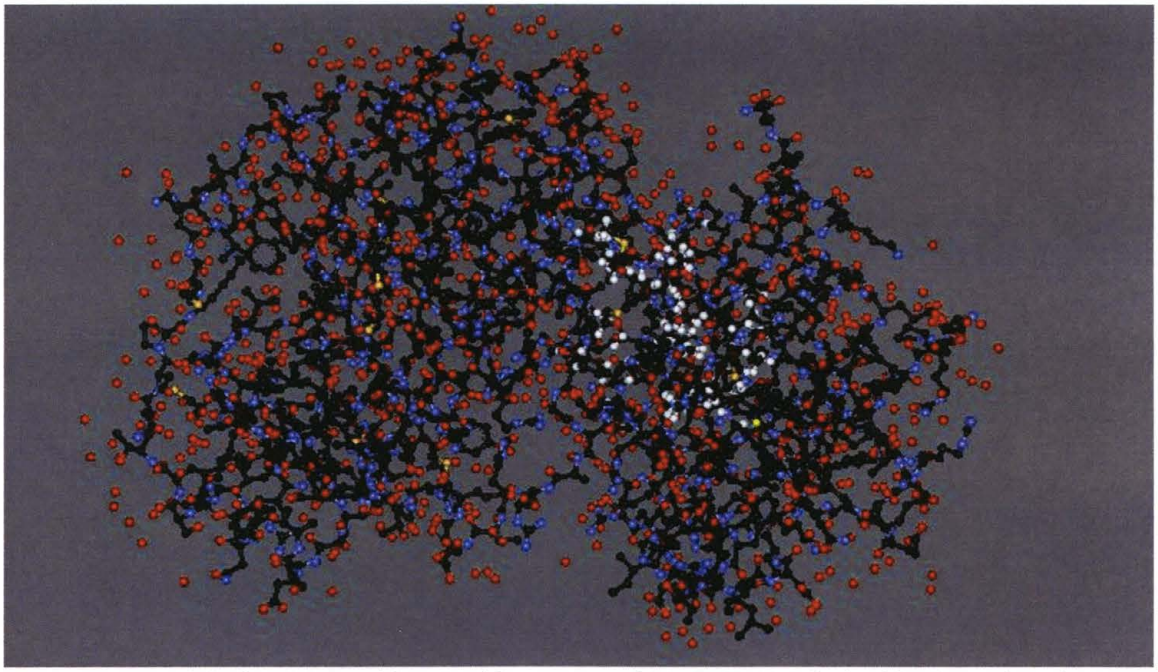

Figure 21. Model of p38 MAP kinase with compound KeAZB-106 docked in the active site.

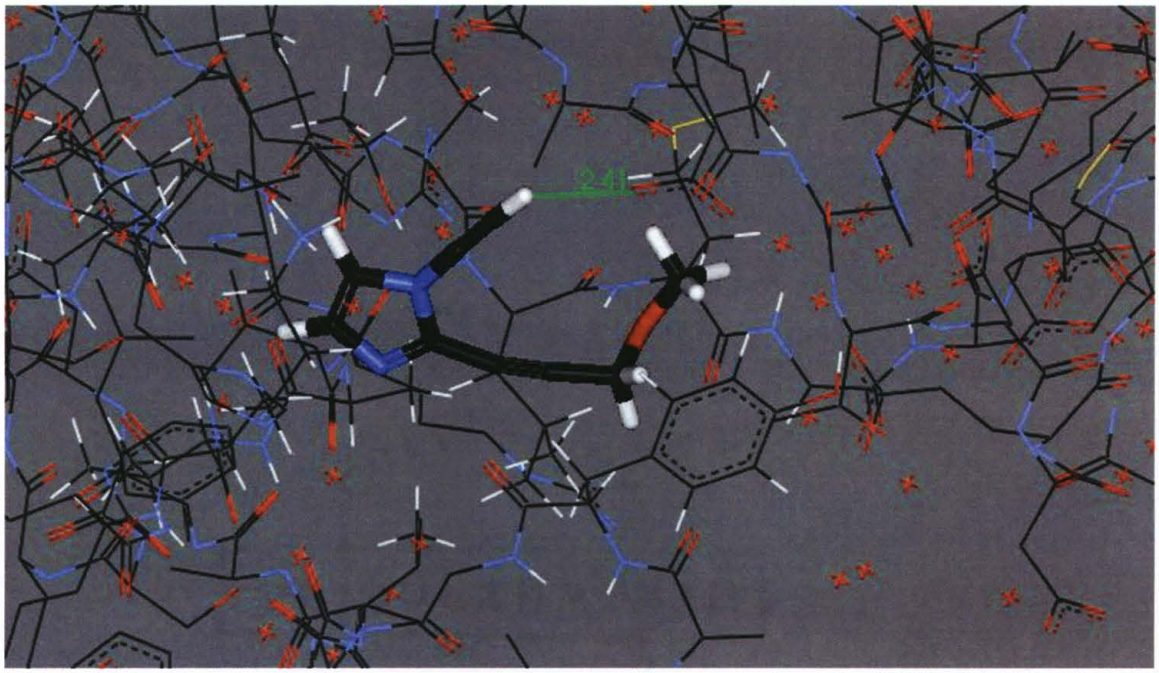

Figure 22. Amino acid residue Asp 168 contained in the active site of p38 MAP kinase forms a hydrogen bond with KeAZB-106.

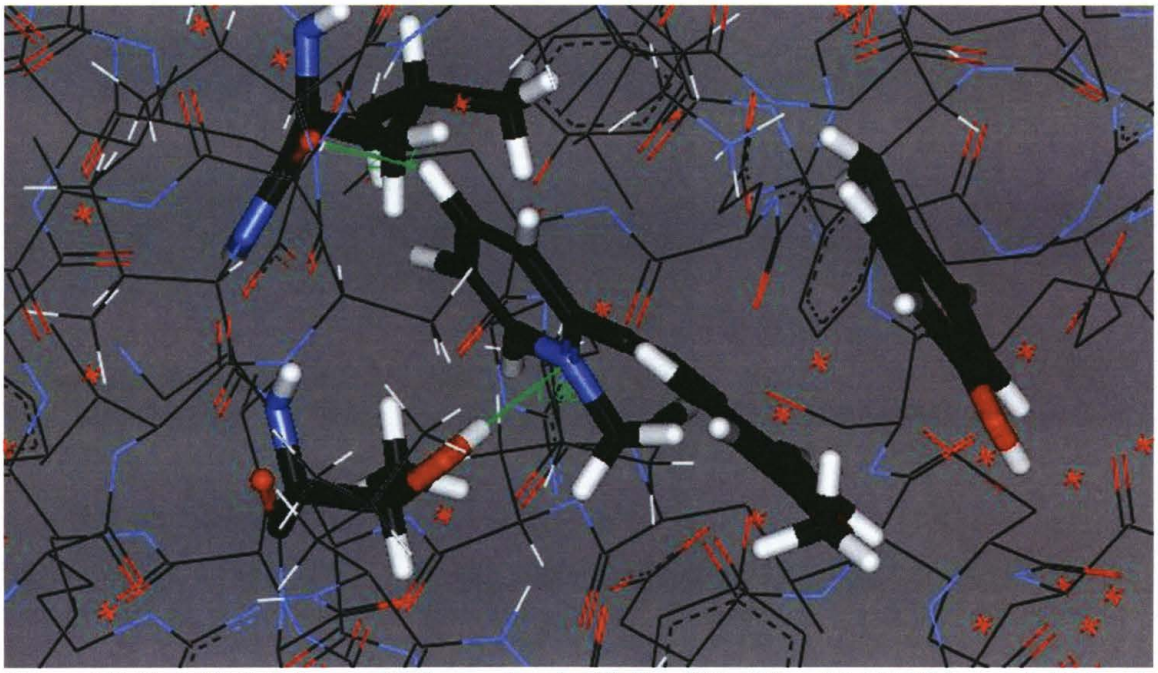

Figure 23. KeAZB-037 forms a hydrogen bond with Tyr 106 of the p38 MAP kinase. Additional

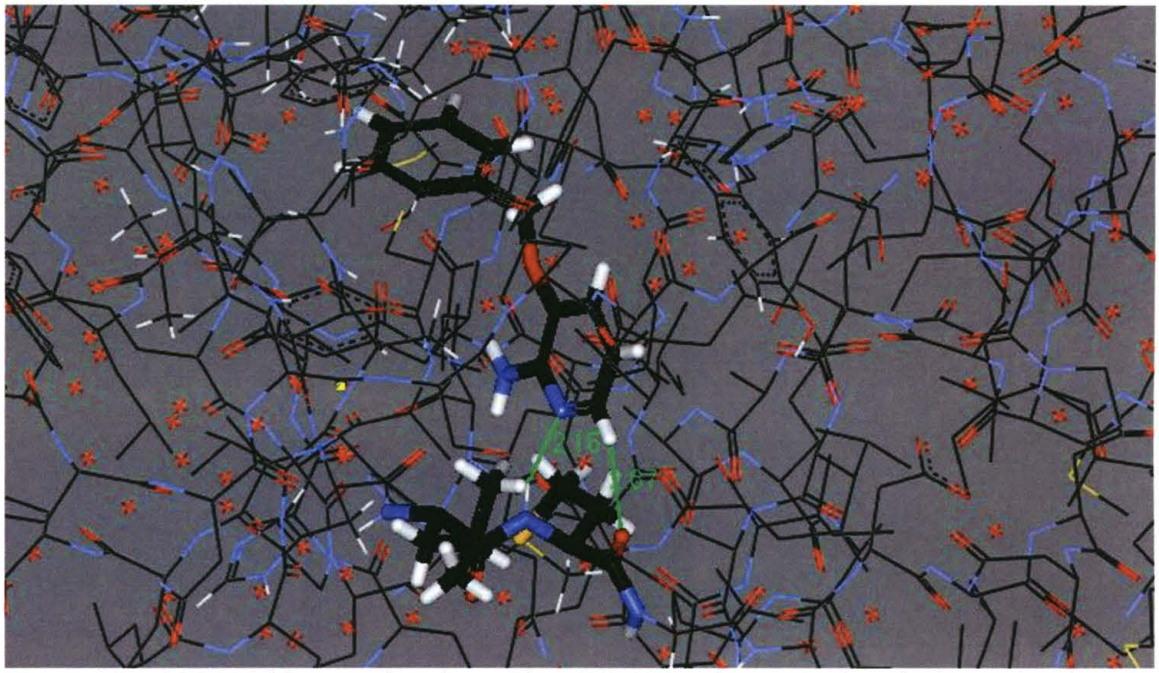

Figure 24. p38 MAP kinase active site residues His 107 and Met 109 form hydrogen bonds to 3-(benzyloxy) pyridine-2-amine.

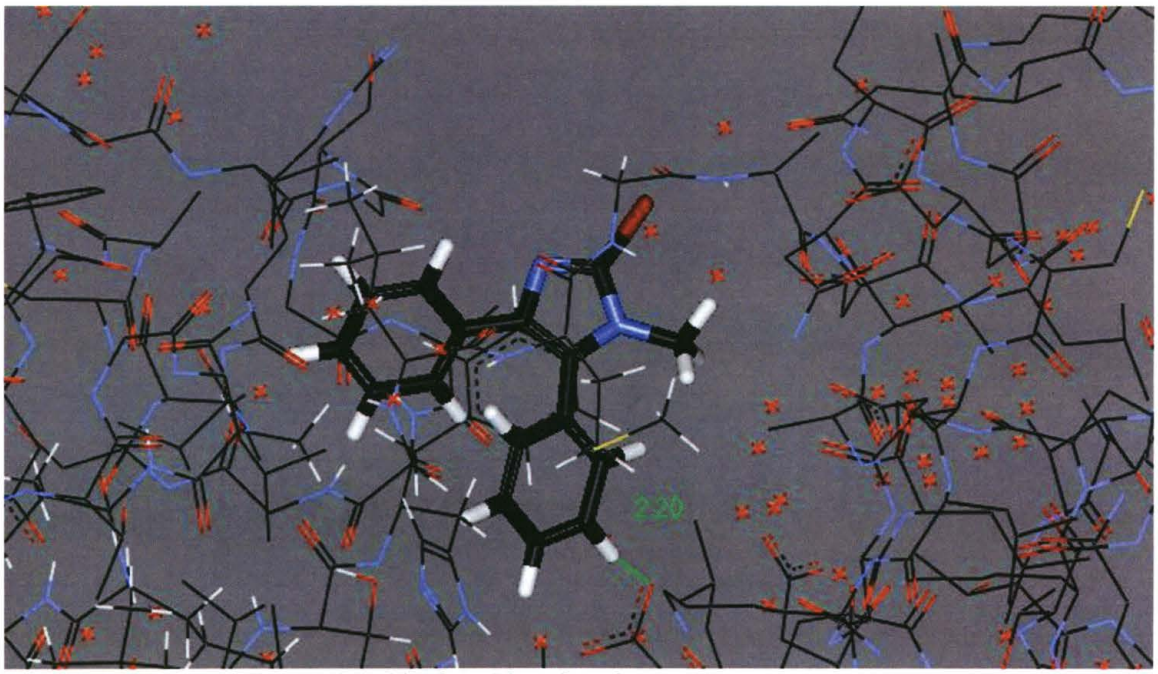

Figure 25. KeAZB-083 modeled in the p38 active site.

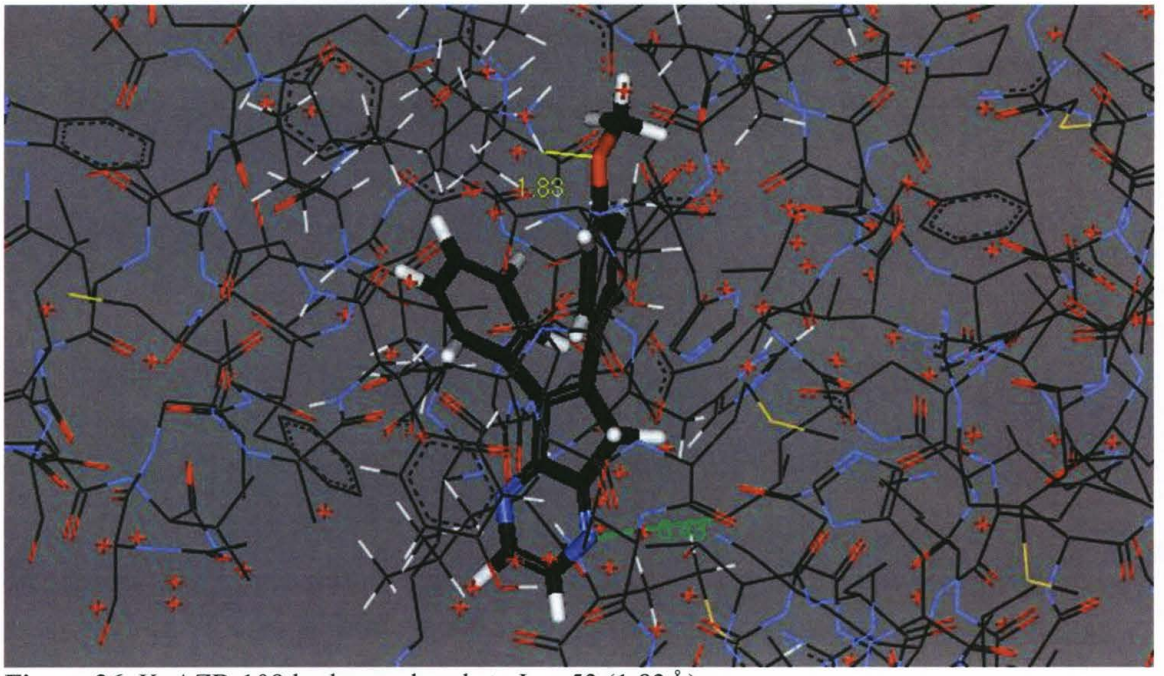

Figure 26. KeAZB-109 hydrogen bonds to Lys 53 (1.83Å).

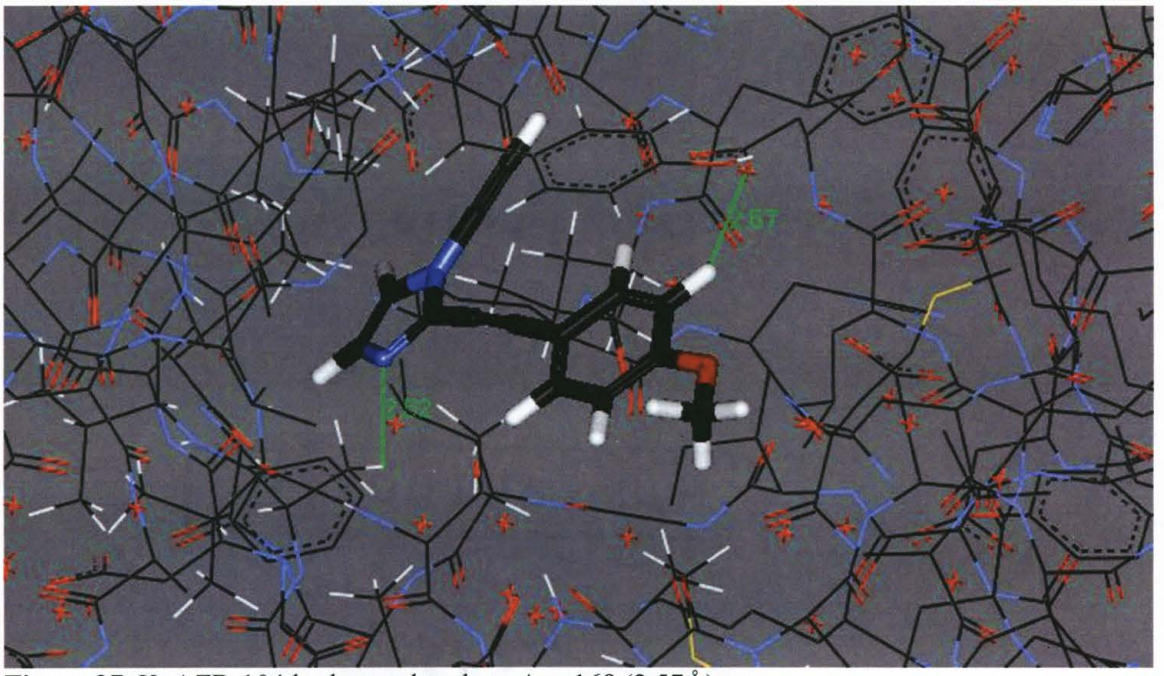

Figure 27. KeAZB-104 hydrogen bonds to Asp 168 (2.57Å).

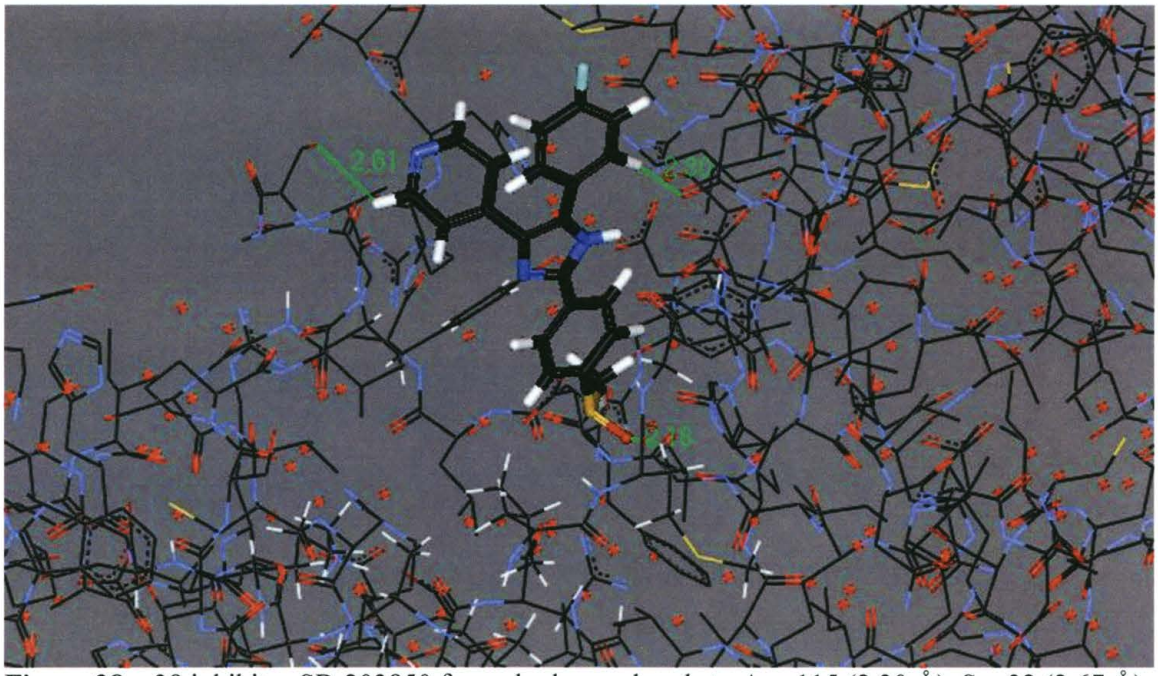

Figure 28. p38 inhibitor SB-203850 forms hydrogen bonds to Asn 115 (2.30 Å), Ser 32 (2.67 Å) and Tyr 35 (2.18 Å).

Summary

Aza-enediynes KeAZB-037 and KeAZB-106 were tested for activity using YCp50 DNA plasmid. This served as a positive control to show that KeAZB-037 and KeAZB-106 were active as DNA cleavage agents. The interaction between a model protein, BSA, and KeAZB-106 and KeAZB-037 was studied by gel electrophoresis. Results indicated that BSA was likely modified by aza-enediynes but the source and the type of modification was not identified. The experiments were followed by MALDI-TOF mass spectrometric analysis of trypsin digested samples. Samples analyzed by MALDI-TOF indicated that there was no difference in the control sample of BSA compared to the incubated BSA:106 samples. This may be due to the large size of BSA compared to that of KeAZB-037 and KeAZB-106, and the low probability of observing an individual modified amino acid in the protein.

Aza-enediynes KeAZB-104 and KeAZB-037 were incubated with bradykinin to determine whether these compounds were capable of producing a covalent peptide modification which would be detectable by MALDI-TOF analysis. Compounds KeAZB-104 and KeAZB-037 both modified bradykinin; however, to further characterize the interaction the peptide fragments produced must be analyzed by tandem mass spectrometry. Future studies will investigate the interaction of these compounds with individual amino acids as well. It is likely that modifications can be detected by mass spectrometry.

In order to investigate a predicted interaction between aza-enediynes and p38, biomolecular interaction analysis was performed. KeAZB-106 was not analyzed but expected to bind p38 according to the modeling experiments performed. However, a

similar molecule, KeAZB-104 showed a small amount of binding to p38. Other aza-enediynes did not show appreciable binding to p38 by biomolecular interaction analysis.

Modeling studies provided supporting evidence for the results determined by biomolecular interaction analysis, except in the case of known p38 inhibitor SB-203580. Molecular modeling simulations do not account for the reorientation that occurs for proteins which follow the induced fit model of binding and this may explain discrepancies observed for inhibitors with bulky substituents.

Future studies include repeating Biacore binding studies at different temperatures to measure the temperature dependence of SB-203580 binding to p38α. A kinetic evaluation would be useful in confirming the affinity of the compound to p38. Analysis of the binding of KeAZB-037, KeAZB-083, KeAZB-104, KeAZB-109, and SB-203580 at various flow rates, concentrations, temperatures, and lengths of injection would provide more complete information about the ability of these compounds to bind to p38. Additionally, molecular modeling is a useful tool for comparing kinetic and binding information. Since constraints were used in the molecular modeling studies of p38 to reduce the time of the dynamics and simulation procedures, the modeling experiments can be redone without constraints. A small peptide such as bradykinin could also be modeled easily, without constraints.

REFERENCES

1. Edo, K.; Mizugaki, M.; Koide, Y.; Seto, J.; Furihara, K.; Otake, N.; Isida, N. *Tetrahedron Lett.* **1985**, *26*, 331-334.

2. Jones, R. R.; Bergman, R.G. *J. Am. Chem. Soc.,* **1972**, *94*, 660-661.

3. Thorson, J. S.; Shen, B.; Whitwam, R. E.; Liu, W.; Li, Y. *Bioorg. Chem.* **1999**, *27*, 172–188.

4. Thorson, J. S.; Sievers, E. L., Ahlert, J.; Shepard, E.; Whitwam, R. E.; Onwueme, K. C.; Ruppen, M. *Curr. Pharm. Des.* **2000**, *6*, 1841–1879.

5. Golik, J.; Dubay, G.; Greonewold, G.; Kawaguchi, H; Konishi, M.; Krishnan, B.; Ohkuma, H.; Saitoh, K.; Doyle, T. W. *J. Am. Chem. Soc.* **1987**, *109*, 3465-3464.

6. Oku, N.; Matsunaga, S.; Fusetani, N. *J. Am. Chem. Soc.,* **2003**, *125*, 2044-2045.

7. Clark, A. E.; Davidson E. R.; Zaleski J. M. *J. Am. Chem. Soc.* **2001**, *123*, 2650-2657.

8. Rule, J. D.; Wilson, S. R.; Moore, J. S. *J. Am. Chem. Soc.*, **2003**, *125*, 12992-12993.

9. Watanabe, C. M. H.; Supekova, L.; Schultz, P. G. *Chem. Biol.*, **2002**, *9*, 245–251.

10. Wang, P; Lee, J.W.; Yu, Y.; Turner, K.; Zou, Y.; Jackson-Cooke, C.K.; Povirk, L.F. *Nucl. Acids Res.*, **2002**, *30*, 2639-2646.

11. Jones, G. B.; Fouad, F. S. *Curr. Pharmaceut. Des.*, **2002**, *8*, 2415-2440.

12. Nicolaou, K.C.; Smith, A.L.; Yue, E. W. *Proc. Nat. Acad. Sci.* **1993**, *90*, 5881-5888.

13. David, W. M.; Kerwin, S. M. *J. Am. Chem. Soc.* **1997**, *119*, 1464-1465.

14. Nadipuram, A.; Kerwin, S. M. *Synlett* **2004**, 1404.

15. David, W. M.; Kumar, D.; Kerwin, S. M. *Bioorg. Med. Chem. Lett.*, **2000**, *10*, 2509-2512.

16. Tuntiwechapikul, W.; David, W. M.; Kumar, D.; Salazar, M.; Kerwin, S. M. *Biochemistry*, **2002**, *41*, 5283-5290.

17. Amine-Khodja, A.; Boulkamh, A.; Boule, P. *Photochem. Photobiol. Sci.* **2004**, *3*, 145-156.

18. Lee, J. C.; Kassis, S.; Kumar, S.; Badger, A.; Adams, J. L. *Pharmacol. Ther.*, **1999**, *82*, 389-397.

19. Kuida, K.; Boucher, D.M. *J. Biochem.* **2004**, *135*, 653-656.

20. Wada, T.; Penninger, J. M. *Oncogene* **2004**, *23*, 2838-284

21. Huang, C.; Jacobson, K.; Schaller, M. D. *J. Cell Sci.* **2004**, *117*, 4619-4628.

22. New, L.; Han, J. *Trends Cardiovasc. Med.*, **1998**, *8*, 220-228.

23. O'Neil, E. A.; Franz, B.; Klatt, T.; Pang, M.; Parsons, J.; Rolando, A.; Williams, H.; Tocci, M.J .; O'Keefe, S. J. *Biochemistry* **1998**, *37*, 13846-13853.

24. Thrumond, R. L.; Wadsworth, S. A.; Schafer, P. H.; Zivin, R. A.; Siekierka, J. L. *Eur. J. Biochem.* **2001**, *268*, 5747-5754.

25. Casper, D.; Bukhtiyarova, M.; Springman, E. B. *Anal. Biochem.* **2004,** 126-136.

26. Janin, J. *Protein Sci.* **2005**, *14*, 278-283.

27. Olson, A. J.; Taylor, P.; Belew, R. K.; Eyck, L. T.; Bailey, M. *SDSC,* www.sdsc.edu/GatherScatter/GSsummer96/gs_summer.html **1996**, 12, No. 3.

28. Hartshorn, M. J.; Murray, C.W.; Cleasby, A.; Frederickson, M.; Tickle, I.J.; Jhoti, H. *J. Med. Chem.* **2005**, *48*, 403-413.

29. Nelson, R. W.; Nedelkov, D.; Tubbs, K. B. *Electrophoresis* **2000**, *21*, 1155-1163.

30. Campbell, J. L.; Kuo, C. *Mol. Cell. Biol.,* **1983**, *3*, 1730-1737.

31. Sun, H.; Ren, P.; Fried, J. R. *Comput. Theor. Polym. Sci.* 1**998,** *8*, 229-46.

32. Sun, H. *J. Phys Chem.* **1998**, *102*, 7338-64.

33. Liang C.; Ewig C. S.; Stouch T. R.; Hagler A. T. *J. Amer. Chem Soc.* **1993**, *115*, 1537-1545.

34. Mayo, S. L.; Olafson B. D.; Goddard, W. A. *J. Phys. Chem.* **1990**, *94*, 8897-8909.

35. Han, J.; Lee, J. D.; Bibbs, L.; Ulevitch, R. J. *Science* **1994**, *265*, 808-811.

36. Cuenda, A.; Rouse, J.; Doza, Y. N.; Meier, R.; Cohen, P.; Gallagher, T.F.; Young, P. R.; Lee, J. C. *FEBS Lett.* **1995**, *364*, 229-233.

VITA

Cristina Gonzales was born in Harlingen, Texas on June 2, 1981, the daughter of Carlos Gonzales and Zulema Garcia. After completing her work at Harlingen High School South, Harlingen, Texas in 1999, she attended Texas State Technical College in Harlingen, Texas. She entered Texas State University in August of 2000. She received the Bachelor of Science Degrees in Biology and Biochemistry from Texas State University-San Marcos in May 2004. In August 2004, she entered the Graduate College of Texas State University-San Marcos.

Permanent Address: 902 Colorado St.

Harlingen, Texas 78550

This thesis was typed by Cristina Gonzales